CERN-ACC-2019-0057

October 2019
giovanni.iadarola@cern.ch
galina.skripka@cern.ch

Beam-induced heat loads on the LHC arc beam screens with different beam and machine configurations: experiments and comparison against simulations

G. Iadarola, G. Skripka, M. Albert, D. Amorim, O. Andujar, S. Antipov, G. Arduini, T. Argyropoulos, B. Bradu, H. Bartosik, C. Bracco, G. Crockford, H. Damerau, R. De Maria, G. P. Di Giovanni, J. C. Dumont, S. Farthoukh, F. Follin, K. Fuchsberger, N. Fuster Martinez, F. Giordano, G. H. Hemelsoet, M. Jaussi, V. Kain, L. Kolbeck, J. Komppula, Y. Le Borgne, K. Li, E. Maclean, L. Mether, E. Metral, G. Papotti, K. Paraschou, T. Persson, S. Redaelli, A. Romano, G. Rumolo, L. Sabato, B. Salvachua Ferrando, B. Salvant, M. Schaumann, E. Shaposhnikova, M. Soderen, M. Solfaroli Camillocci, R. Suykerbuyk, O. Sveen, L. Tavian, L. Teofili, H. Timko, R. Tomas Garcia, G. Trad, J. Uythoven, S. Uznanski, D. Valuch, F. Velotti, D. Walsh, J. Wenninger, E. Wulff

CERN, CH-1211 Geneva, Switzerland

Keywords: LHC, arcs, heat load, electron cloud, MD2484, MD3295, MD3296, MD3297, MD3298, MD3300, MD4203

Abstract

Electron cloud (e-cloud) effects are among the main performance limitations for the operation of the Large Hadron Collider (LHC) with 25 ns bunch spacing. A large number of electrons impacting on the beam screens of the superconducting magnets induces significant heat load, reaching values close to the full cooling capacity available from the cryogenic system. A number of Machine Development (MD) sessions in 2018 was dedicated to characterizing the heat load as a function of beam and machine parameters, investigating in particular its distribution along the ring and its dependence on the filling pattern, bunch population and bunch length.

The main results of these measurements have been compared against simulations performed with the PyECLOUD code in order to validate the underlying model.

Contents

1 Introduction **3**

2 Experimental characterization of the arc heat loads **5**
2.1 Distribution along the ring and measurements with one circulating beam . . 5
2.1.1 Instrumented half-cells 13
2.2 Dependence on the number of circulating bunches 18
2.3 Dependence on the bunch intensity 18
2.4 Dependence on the bunch length 22
2.5 Test with high-intensity 8b+4e beams 24
2.6 Additional tests 31
2.6.1 Effect of the field in the spool-piece correctors 31
2.6.2 Effect of orbit bumps 32

3 Comparisons against models and simulations **38**
3.1 Comparison of heat load data against e-cloud simulations 39

4 Conclusions **47**

1 Introduction

During Run 2, beams with 25 ns bunch spacing were routinely used for proton physics operation at the LHC. With this bunch spacing, electron cloud (e-cloud) effects are significantly more severe than with the 50 ns spacing, which had been used for luminosity production in Run 1. Beam-induced surface conditioning (also called "scrubbing"), allowed mitigating the e-cloud formation enough for an effective exploitation of 25 ns beams in physics operation. Nevertheless, even after years of conditioning of the beam screens, e-cloud effects remain very visible, affecting beam stability and beam quality preservation, and generating a significant heat load on the beam screens of the superconducting magnets [1, 2].

These heat loads are much larger than expected from impedance and synchrotron radiation and vary significantly from arc to arc, as shown in Fig. 1. For some sectors the heat load is close to the cooling capacity available from the cryogenics. This poses concerns for the foreseen High-Luminosity LHC project, which relies on a two-fold increase of the beam intensity [3].

The differences in heat load among the arcs are not expected as the eight arcs are by design identical. Moreover, they were not always present. A test period with 25 ns beams took place at the end of Run 1, in 2012. The heat loads measured during that period can be directly compared against Run 2 data, as the measurement system was largely unchanged and the beam conditions were very similar [4]. A comparison between similar fills performed before and after LS1 is shown in Fig. 2. It is evident that the differences among arcs appeared only after LS1, during which all arcs were warmed up to room temperature and exposed to air. It is possible to notice that still in 2017, after multiple years of conditioning of the beam

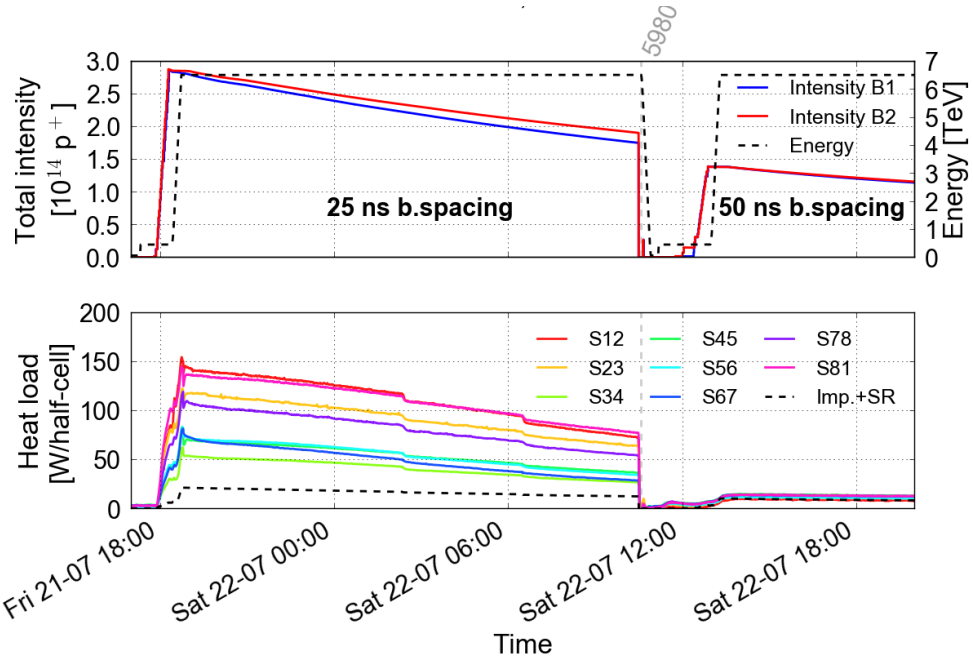

Figure 1: Intensities of the two LHC beams (top) and evolution of the heat loads in the eight LHC arcs (bottom) during two consecutive fills with different bunch spacing. The expected load from impedance and synchrotron radiation is indicated by the dashed curve.

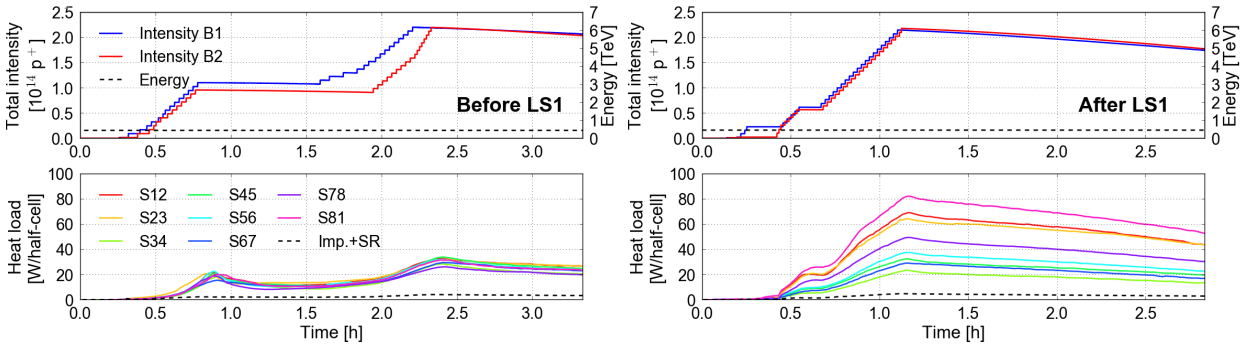

Figure 2: Beam intensities (top) and heat loads in the eight LHC arcs (bottom) during two fills with the same filling pattern in 2012 (left, fill 3438) and in 2017 (right, fill 5814).

screens, the heat load in the high-load arcs is four times larger than before LS1. So far, no difference in the activities conducted during LS1 in the eight arcs could be identified, which could explain this different behaviour in terms of heat load. A dedicated interdepartmental task force has been formed to investigate this issue [5].

In 2018, as part of this program, several machine development (MD) sessions, listed in Table 1, were dedicated to tests aiming at characterizing the heat loads on the LHC beam screens, using different beam and machine configurations. This document summarizes these studies and compares the main results against models and numerical simulations.

MD #	Start	Fill #	Title
3297	05:00, 13-06-2018	6788	Heat load measurements with orbit bumps in the arcs
3296	11:00, 13-06-2018	6786, 6787	Impact of spool-piece correctors on heat loads
3300	18:00, 13-06-2018 05:00, 24-07-2018 04:00, 13-09-2018	6786, 6789, 6790 6968 7160	Heat load measurements with different bunch intensity
3295	21:00, 23-07-2018	6966, 6967	Heat load measurements with a single circulating beam
3298	00:00, 13-09-2018	7157	Heat load measurements with different bunch lengths
4203	13:00, 25-10-2018	7353, 7354, 7355, 7356	Heat load measurements with high bunch intensity (trains of 12b)
2484	16:00, 26-10-2018	7365, 7366	Electron cloud studies with high intensity 8b+4e beams

Table 1: Summary of MD sessions dedicated to heat load studies in 2018

2 Experimental characterization of the arc heat loads

The following subsections describe the methods and the results of different measurements performed to characterize the beam-induced heat loads on the arc beam screens.

2.1 Distribution along the ring and measurements with one circulating beam

During standard physics fills with 25 ns bunch spacing, differences in heat load are observed not only among the different arcs, but also among different cells within the same arc as illustrated by the green bars in Figs. 6 - 9. In normal operation it is not possible to identify the heat load produced by each of the circulating beams, due to the fact that, in regular arc cells, the individual cooling channels are not equipped with temperature probes.

During the MD3295 session, a dedicated test was performed in order to measure the heat loads generated by the two beams individually. As illustrated in Fig. 3, this was done in two consecutive fills, the first with 2556 bunches in Ring 1 and 12 bunches in Ring 2 and the second with 12 bunches in Ring 1 and 2556 bunches in Ring 2. A short train of 12 bunches had to be injected in the otherwise empty ring since some beam needs to be present in both rings in order to correctly perform the energy ramp in the standard machine configuration. The same filling scheme used for the LHC luminosity production in 2018 was employed also during this MD. The scheme is made of injections of 3×48 bunches. The two fills were also

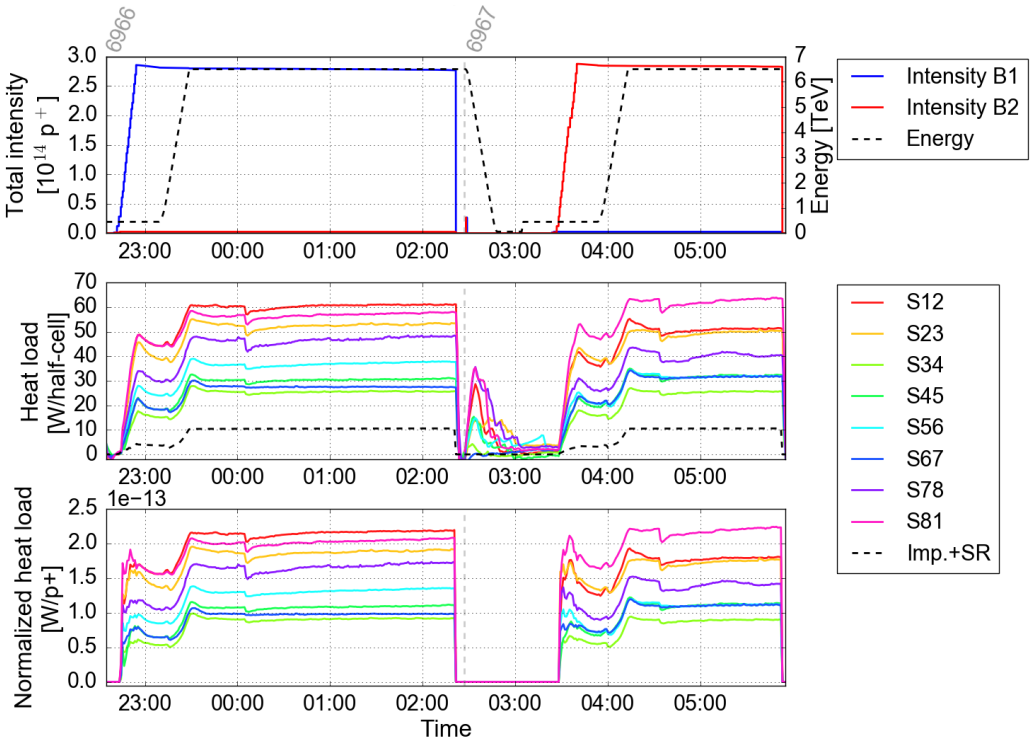

Figure 3: Beam intensities and heat loads measured during the test fills with a single circulating beam (fills 6966 and 6967).

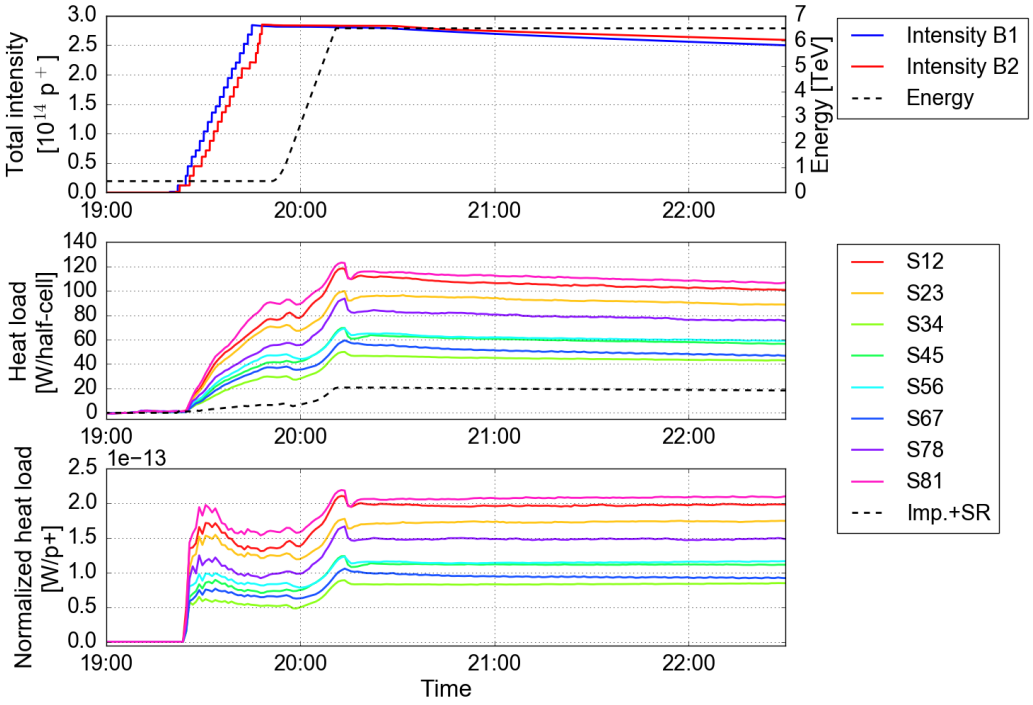

Figure 4: Beam intensities and heat loads measured during a typical physics fill (fill 6961).

used to study beam lifetime evolution with one circulating beam [6].

The average heat loads measured in the arcs during the test are shown in Fig. 3 and can be compared with the ones measured with two circulating beams during typical physics fill, shown in Fig. 4. Large differences among arcs are observed also with one circulating beam.

Figure 5 shows a further comparison of the heat loads measured with Beam 1 alone (in blue), with Beam 2 alone (in red) and with two circulating beams (in green). It is possible to observe that the measurements performed with one beam add up almost exactly to those performed with two beams. This provides a validation of the linearity of the measurement given by the cryogenic system. The plot also shows that within some arcs, differences are visible between the heat loads generated by Beam 1 and Beam 2 separately.

A similar comparison has been performed also at a cell-by-cell level and is shown in Figs. 6 - 9. On several cells (e.g. 33R1-7, 21L2-3, 31L3-3, 23L3-3) a very large difference is observed between the heat loads generated by Beam 1 and Beam 2. A significant discrepancy between the sum of heat loads measured with one beam and the heat loads measured with two beams together is observed only in a very small number of cells, most likely due to issues with the cryogenic measurement.

In Fig. 10 the heat loads produced by the two beams are plotted against each other. No evident correlation is observed between the heat load measured with Beam 1 alone and with Beam 2 alone.

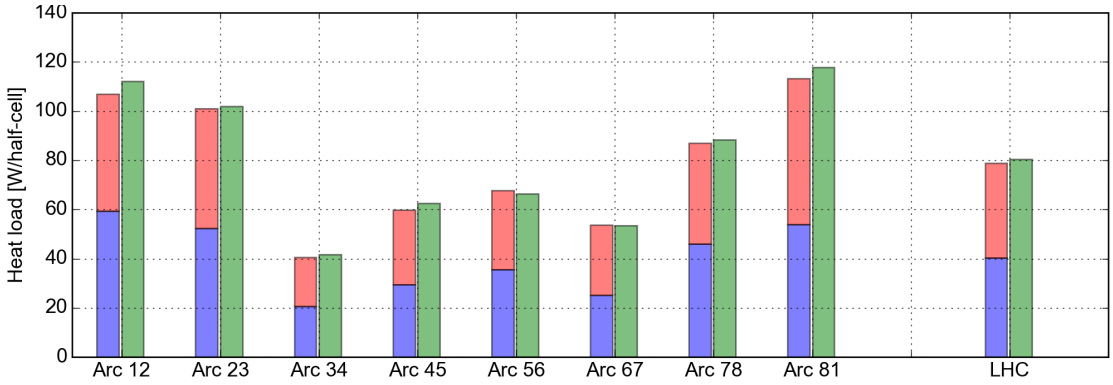

Fill	6966	6967	6961
Started on	23 Jul 2018 22:33	24 Jul 2018 02:27	22 Jul 2018 18:22
T_sample [h]	2.20	2.80	2.00
Energy [GeV]	6499	6499	6499
N_bunches (B1/B2)	2556/24	24/2556	2556/2556
Intensity (B1/B2) [p]	2.79e14/2.40e12	2.39e12/2.84e14	2.79e14/2.83e14
Bun.len. (B1/B2) [ns]	1.07/1.06	1.07/1.10	1.11/1.10
H.L. exp. imped. [W]	4.52	4.49	8.77
H.L. exp. synrad [W]	5.99	6.09	11.96
H.L. exp. imp.+SR [W/p+]	3.73e-14	3.70e-14	3.69e-14
T_nobeam [h]	0.50	1.30	0.90

Figure 5: Average heat loads measured in the LHC arcs with only Beam 1 (in blue), only Beam 2 (in red) and with both beams together (in green). Bottom: table with different relevant quantities at the time of the three measurements.

Arc 12

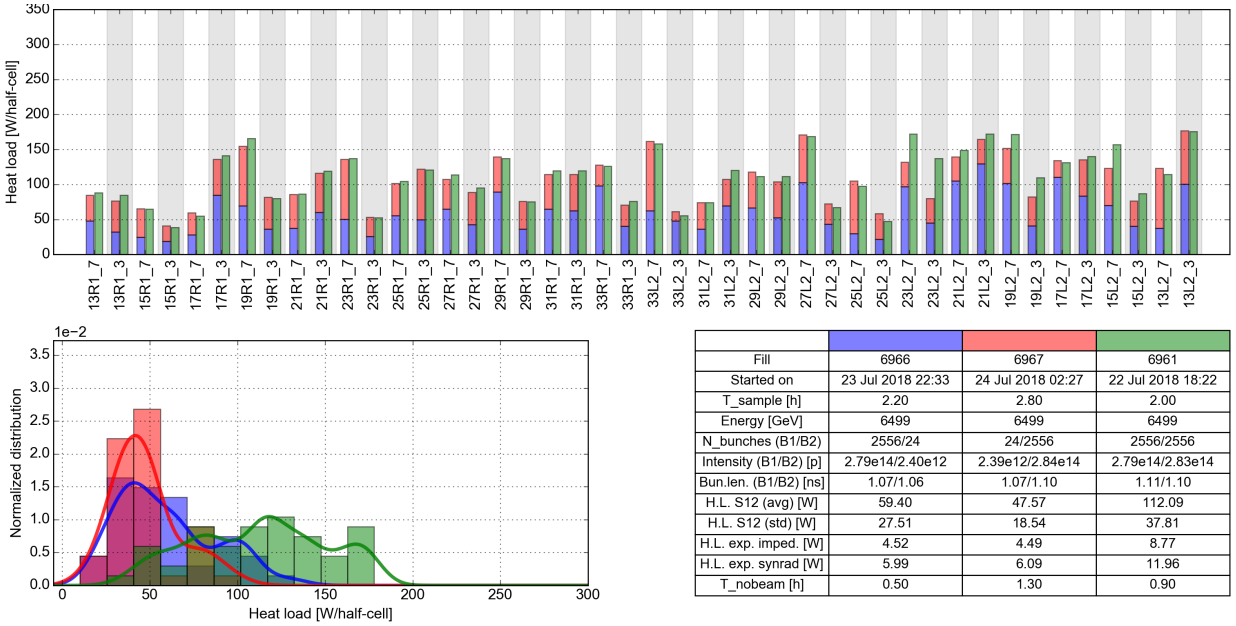

Fill	6966	6967	6961
Started on	23 Jul 2018 22:33	24 Jul 2018 02:27	22 Jul 2018 18:22
T_sample [h]	2.20	2.80	2.00
Energy [GeV]	6499	6499	6499
N_bunches (B1/B2)	2556/24	24/2556	2556/2556
Intensity (B1/B2) [p]	2.79e14/2.40e12	2.39e12/2.84e14	2.79e14/2.83e14
Bun.len. (B1/B2) [ns]	1.07/1.06	1.07/1.10	1.11/1.10
H.L. S12 (avg) [W]	59.40	47.57	112.09
H.L. S12 (std) [W]	27.51	18.54	37.81
H.L. exp. imped. [W]	4.52	4.49	8.77
H.L. exp. synrad [W]	5.99	6.09	11.96
T_nobeam [h]	0.50	1.30	0.90

Arc 23

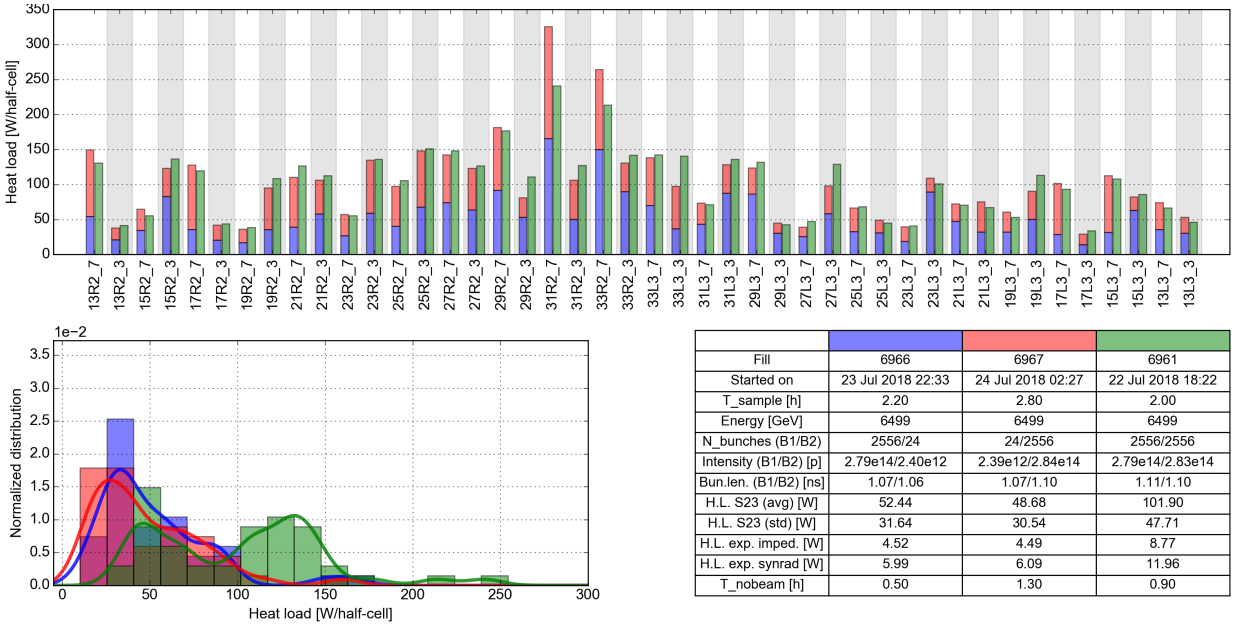

Fill	6966	6967	6961
Started on	23 Jul 2018 22:33	24 Jul 2018 02:27	22 Jul 2018 18:22
T_sample [h]	2.20	2.80	2.00
Energy [GeV]	6499	6499	6499
N_bunches (B1/B2)	2556/24	24/2556	2556/2556
Intensity (B1/B2) [p]	2.79e14/2.40e12	2.39e12/2.84e14	2.79e14/2.83e14
Bun.len. (B1/B2) [ns]	1.07/1.06	1.07/1.10	1.11/1.10
H.L. S23 (avg) [W]	52.44	48.68	101.90
H.L. S23 (std) [W]	31.64	30.54	47.71
H.L. exp. imped. [W]	4.52	4.49	8.77
H.L. exp. synrad [W]	5.99	6.09	11.96
T_nobeam [h]	0.50	1.30	0.90

Figure 6: Cell-by-cell heat loads with only Beam 1 (blue), only Beam 2 (red) and with the two beams together (green) for the arcs 12 and 23. Histograms of the load distribution and a table with different relevant quantities at the time of the measurements are also shown.

Arc 34

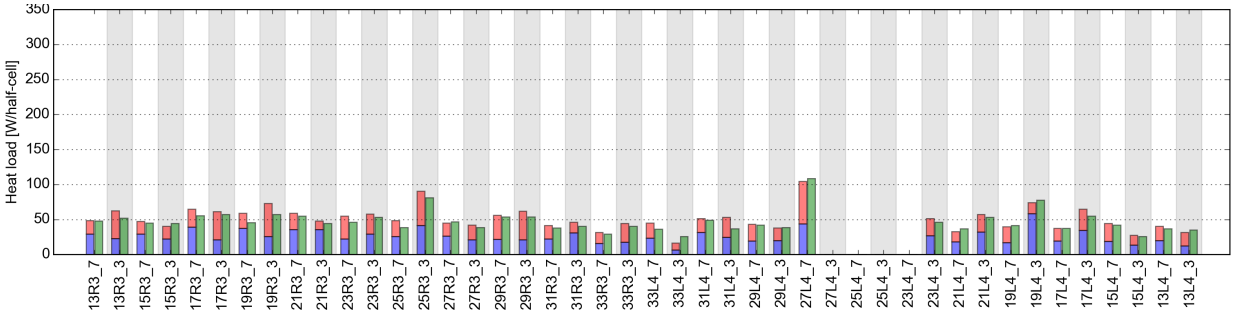

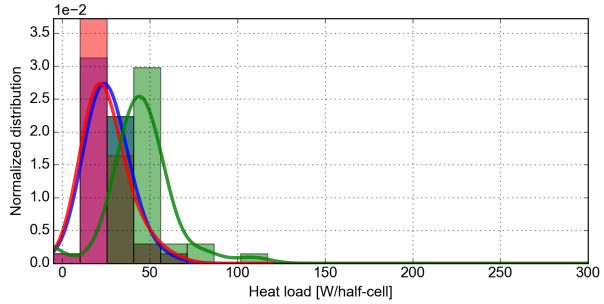

Fill	6966	6967	6961
Started on	23 Jul 2018 22:33	24 Jul 2018 02:27	22 Jul 2018 18:22
T_sample [h]	2.20	2.80	2.00
Energy [GeV]	6499	6499	6499
N_bunches (B1/B2)	2556/24	24/2556	2556/2556
Intensity (B1/B2) [p]	2.79e14/2.40e12	2.39e12/2.84e14	2.79e14/2.83e14
Bun.len. (B1/B2) [ns]	1.07/1.06	1.07/1.10	1.11/1.10
H.L. S34 (avg) [W]	20.66	20.02	41.79
H.L. S34 (std) [W]	18.99	19.06	22.32
H.L. exp. imped. [W]	4.52	4.49	8.77
H.L. exp. synrad [W]	5.99	6.09	11.96
T_nobeam [h]	0.50	1.30	0.90

Arc 45

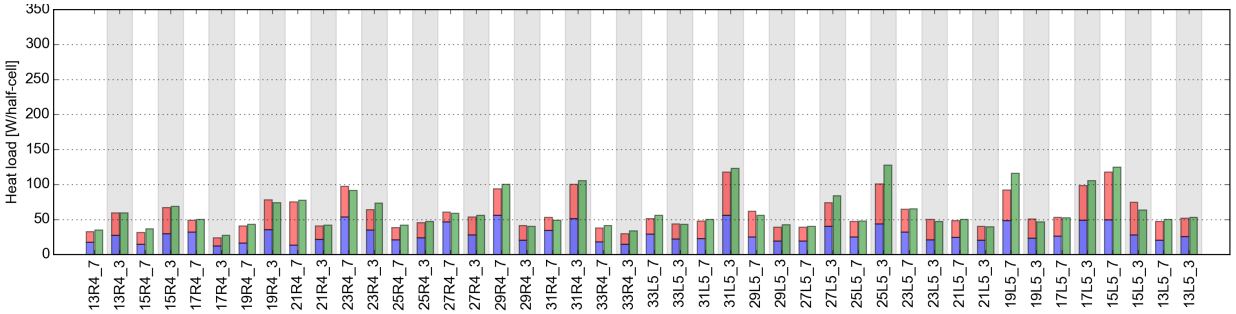

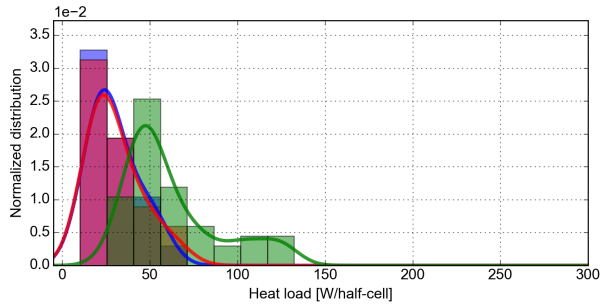

Fill	6966	6967	6961
Started on	23 Jul 2018 22:33	24 Jul 2018 02:27	22 Jul 2018 18:22
T_sample [h]	2.20	2.80	2.00
Energy [GeV]	6499	6499	6499
N_bunches (B1/B2)	2556/24	24/2556	2556/2556
Intensity (B1/B2) [p]	2.79e14/2.40e12	2.39e12/2.84e14	2.79e14/2.83e14
Bun.len. (B1/B2) [ns]	1.07/1.06	1.07/1.10	1.11/1.10
H.L. S45 (avg) [W]	29.54	30.31	62.44
H.L. S45 (std) [W]	12.31	14.04	26.57
H.L. exp. imped. [W]	4.52	4.49	8.77
H.L. exp. synrad [W]	5.99	6.09	11.96
T_nobeam [h]	0.50	1.30	0.90

Figure 7: Cell-by-cell heat loads with only Beam 1 (blue), only Beam 2 (red) and with the two beams together (green) for the arcs 34 and 45. Histograms of the load distribution and a table with different relevant quantities at the time of the measurements are also shown.

Arc 56

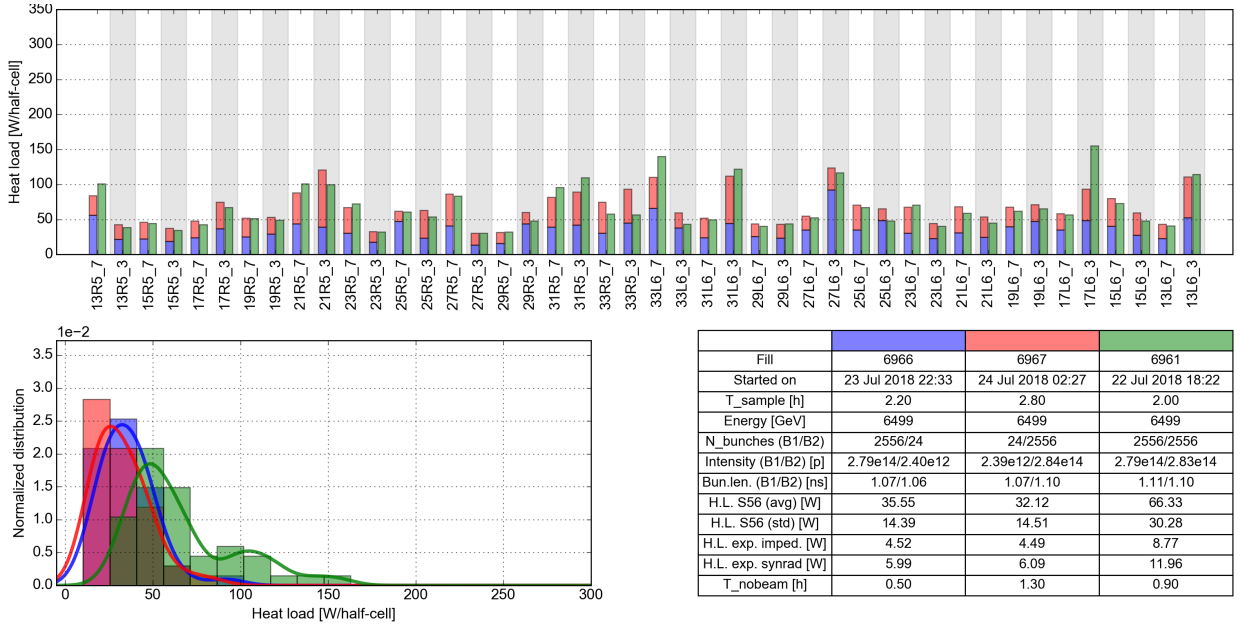

Fill	6966	6967	6961
Started on	23 Jul 2018 22:33	24 Jul 2018 02:27	22 Jul 2018 18:22
T_sample [h]	2.20	2.80	2.00
Energy [GeV]	6499	6499	6499
N_bunches (B1/B2)	2556/24	24/2556	2556/2556
Intensity (B1/B2) [p]	2.79e14/2.40e12	2.39e12/2.84e14	2.79e14/2.83e14
Bun.len. (B1/B2) [ns]	1.07/1.06	1.07/1.10	1.11/1.10
H.L. S56 (avg) [W]	35.55	32.12	66.33
H.L. S56 (std) [W]	14.39	14.51	30.28
H.L. exp. imped. [W]	4.52	4.49	8.77
H.L. exp. synrad [W]	5.99	6.09	11.96
T_nobeam [h]	0.50	1.30	0.90

Arc 67

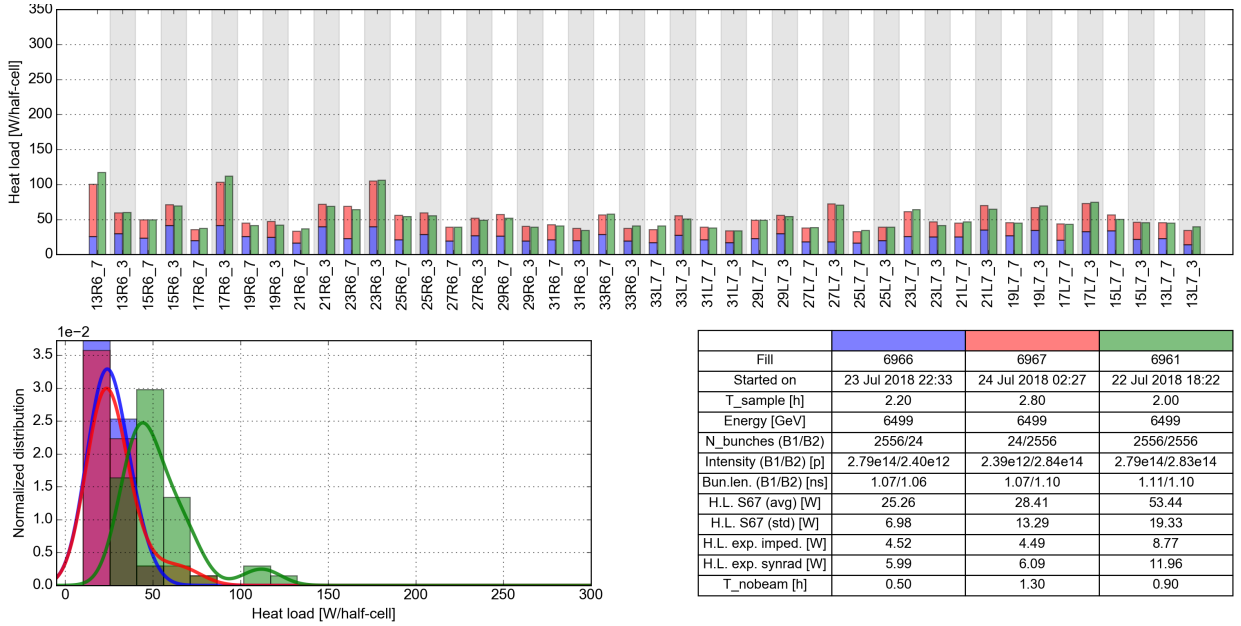

Fill	6966	6967	6961
Started on	23 Jul 2018 22:33	24 Jul 2018 02:27	22 Jul 2018 18:22
T_sample [h]	2.20	2.80	2.00
Energy [GeV]	6499	6499	6499
N_bunches (B1/B2)	2556/24	24/2556	2556/2556
Intensity (B1/B2) [p]	2.79e14/2.40e12	2.39e12/2.84e14	2.79e14/2.83e14
Bun.len. (B1/B2) [ns]	1.07/1.06	1.07/1.10	1.11/1.10
H.L. S67 (avg) [W]	25.26	28.41	53.44
H.L. S67 (std) [W]	6.98	13.29	19.33
H.L. exp. imped. [W]	4.52	4.49	8.77
H.L. exp. synrad [W]	5.99	6.09	11.96
T_nobeam [h]	0.50	1.30	0.90

Figure 8: Cell-by-cell heat loads with only Beam 1 (blue), only Beam 2 (red) and with the two beams together (green) for the arcs 56 and 67. Histograms of the load distribution and a table with different relevant quantities at the time of the measurements are also shown.

Arc 78

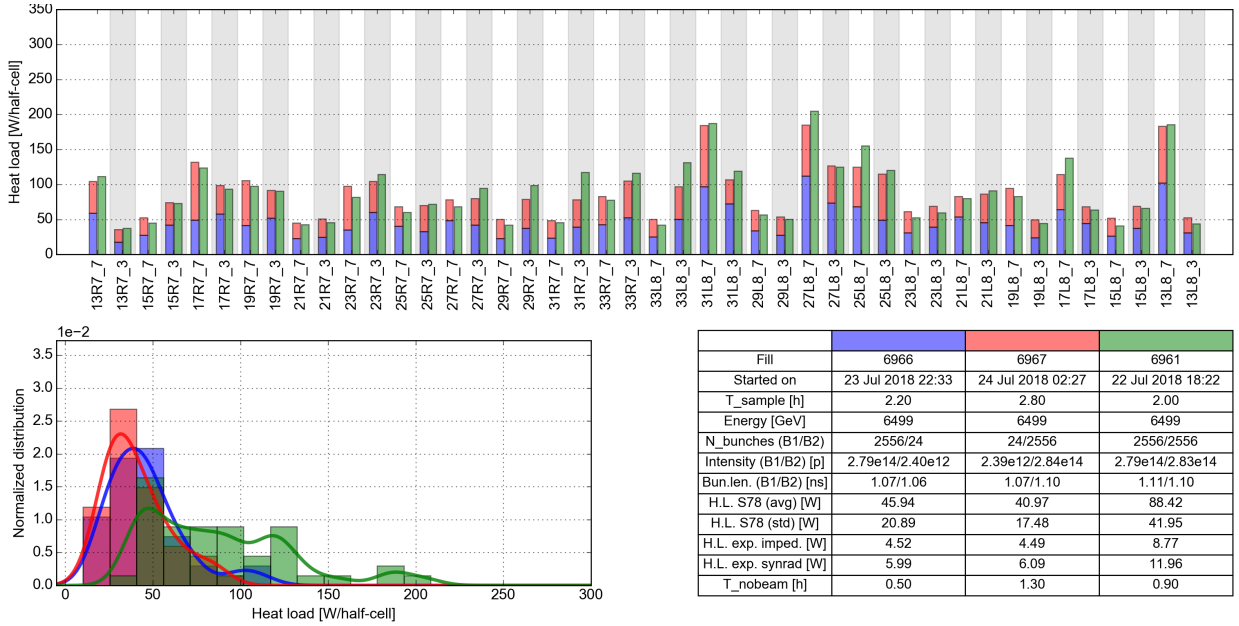

Fill	6966	6967	6961
Started on	23 Jul 2018 22:33	24 Jul 2018 02:27	22 Jul 2018 18:22
T_sample [h]	2.20	2.80	2.00
Energy [GeV]	6499	6499	6499
N_bunches (B1/B2)	2556/24	24/2556	2556/2556
Intensity (B1/B2) [p]	2.79e14/2.40e12	2.39e12/2.84e14	2.79e14/2.83e14
Bun.len. (B1/B2) [ns]	1.07/1.06	1.07/1.10	1.11/1.10
H.L. S78 (avg) [W]	45.94	40.97	88.42
H.L. S78 (std) [W]	20.89	17.48	41.95
H.L. exp. imped. [W]	4.52	4.49	8.77
H.L. exp. synrad [W]	5.99	6.09	11.96
T_nobeam [h]	0.50	1.30	0.90

Arc 81

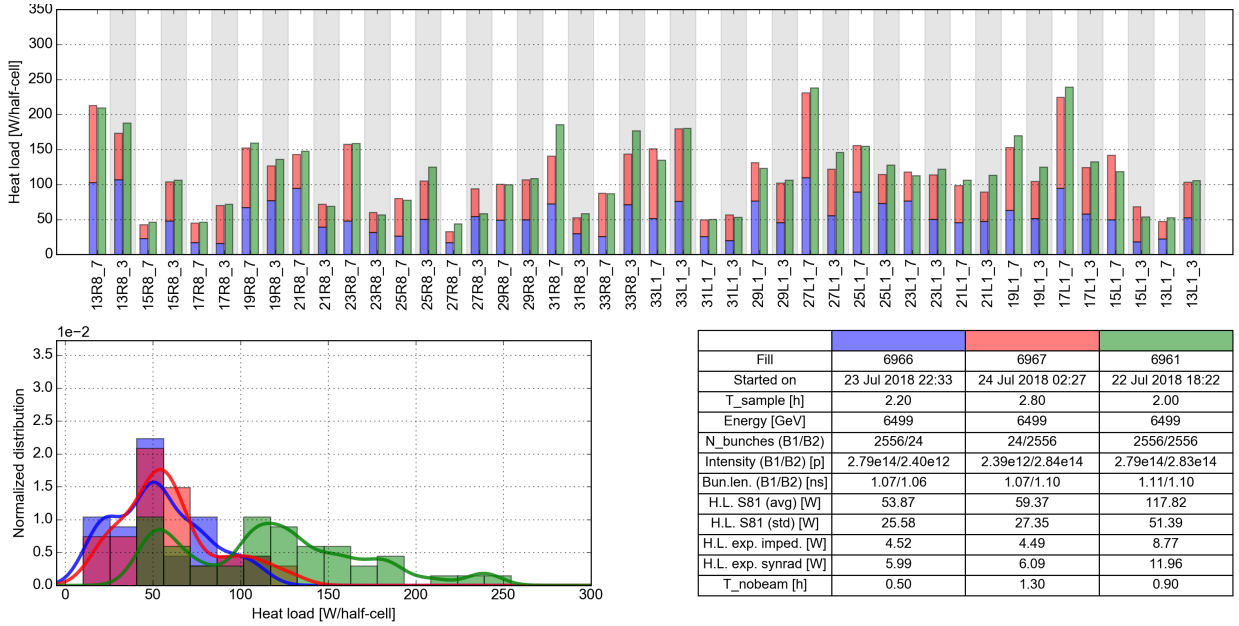

Fill	6966	6967	6961
Started on	23 Jul 2018 22:33	24 Jul 2018 02:27	22 Jul 2018 18:22
T_sample [h]	2.20	2.80	2.00
Energy [GeV]	6499	6499	6499
N_bunches (B1/B2)	2556/24	24/2556	2556/2556
Intensity (B1/B2) [p]	2.79e14/2.40e12	2.39e12/2.84e14	2.79e14/2.83e14
Bun.len. (B1/B2) [ns]	1.07/1.06	1.07/1.10	1.11/1.10
H.L. S81 (avg) [W]	53.87	59.37	117.82
H.L. S81 (std) [W]	25.58	27.35	51.39
H.L. exp. imped. [W]	4.52	4.49	8.77
H.L. exp. synrad [W]	5.99	6.09	11.96
T_nobeam [h]	0.50	1.30	0.90

Figure 9: Cell-by-cell heat loads with only Beam 1 (blue), only Beam 2 (red) and with the two beams together (green) for the arcs 78 and 81. Histograms of the load distribution and a table with different relevant quantities at the time of the measurements are also shown.

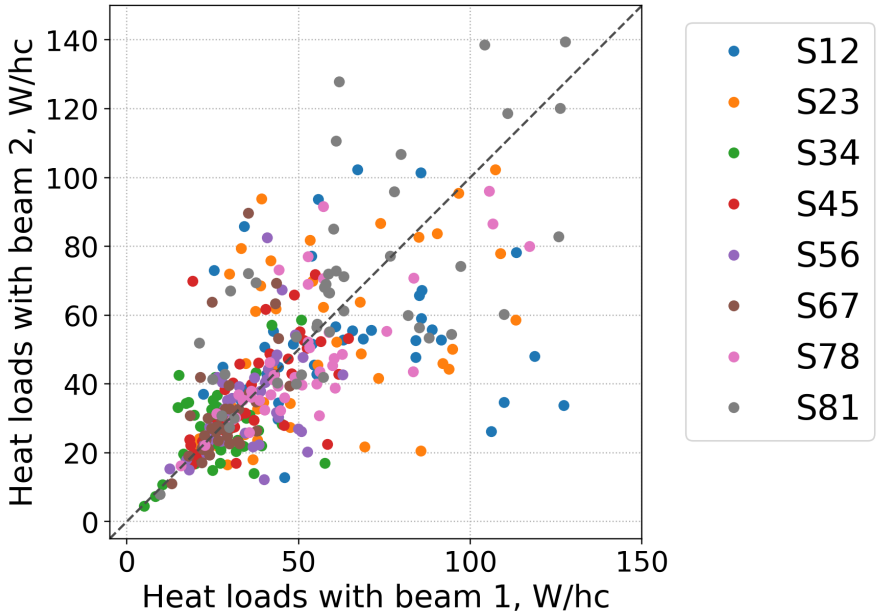

Figure 10: Heat loads measured in all the LHC half-cells with only Beam 1 and only Beam 2.

2.1.1 Instrumented half-cells

Four half-cells in the LHC arcs have been instrumented with additional thermal probes on the cooling tubes, at each interconnection between consecutive magnets. These allow measuring the heat load on the individual magnets.

The heat load measured on the dipole magnets in these instrumented cells during a typical luminosity fill in 2018 is reported in Figs. 11 - 14. It is evident that large differences in heat load are present even among magnets of the same type within a given half-cell.

In particular, in the half-cell 31L2 located in the arc 12, the "D4" dipole, installed during the Extended Year-End Technical Stop in 2017, shows a very low heat load, compatible with the expectation from impedance and synchrotron radiation models. The "D2" and "D3" magnets, instead, show much larger heat loads due to a strong contribution from e-cloud effects.

The other instrumented half-cells are located in the Arc 45. Most of the magnets in these cells show low heat loads, with the exception of the "D3" dipole in the half-cell 33L5 and the "D2" dipole in the half-cell 13L5.

Figure 15 shows the heat load measured in the quadrupole magnets of the instrumented cell during the same fill. Most of them have rather low heat loads with the notable exception of the quadrupole in the half-cell 31L2, which shows very high heat load at injection energy. The heat load in this magnet decreases significantly during the energy ramp. This behavior is driven by the change of the magnetic fields and is found to be compatible with e-cloud build-up simulations [7].

In most of the instrumented dipoles it is possible to measure independently the heat loads from the two beams. Figures 16 - 18 show the heat load measured on the two apertures for the dipoles having the largest heat loads. We notice that for the 31L2-D3 magnet the heat load is generated in a similar way by both beams while for the 31L2-D2 and for the 33L5-D3 the heat load is mainly induced by Beam 1.

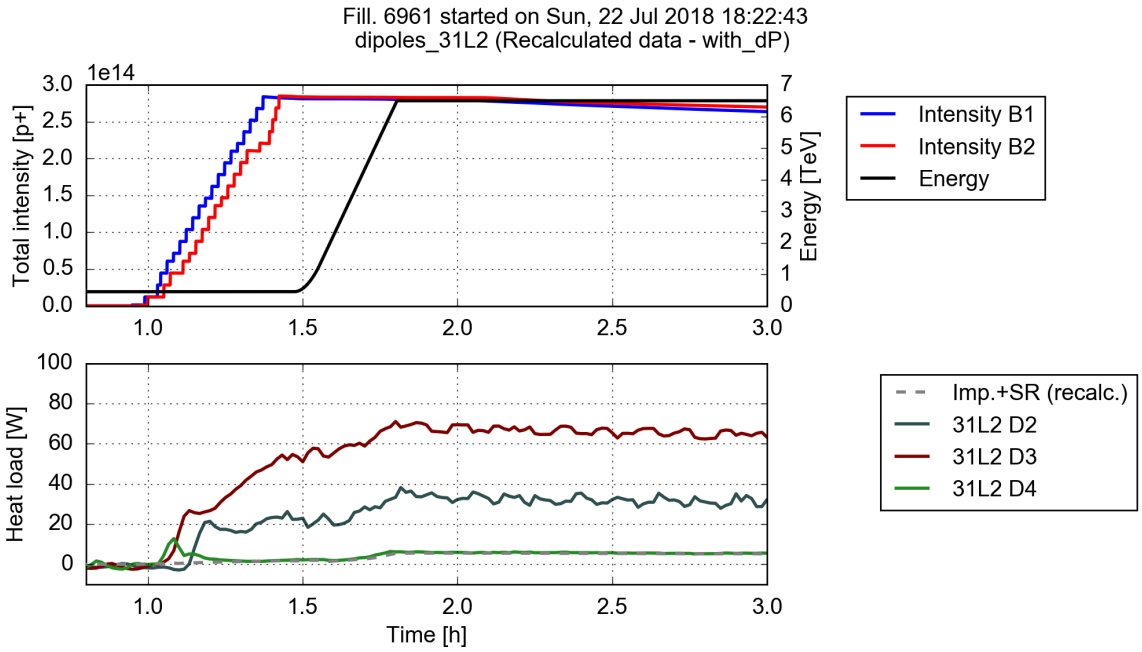

Figure 11: Heat loads on the beam screens of the instrumented dipoles in the half-cell 31L2.

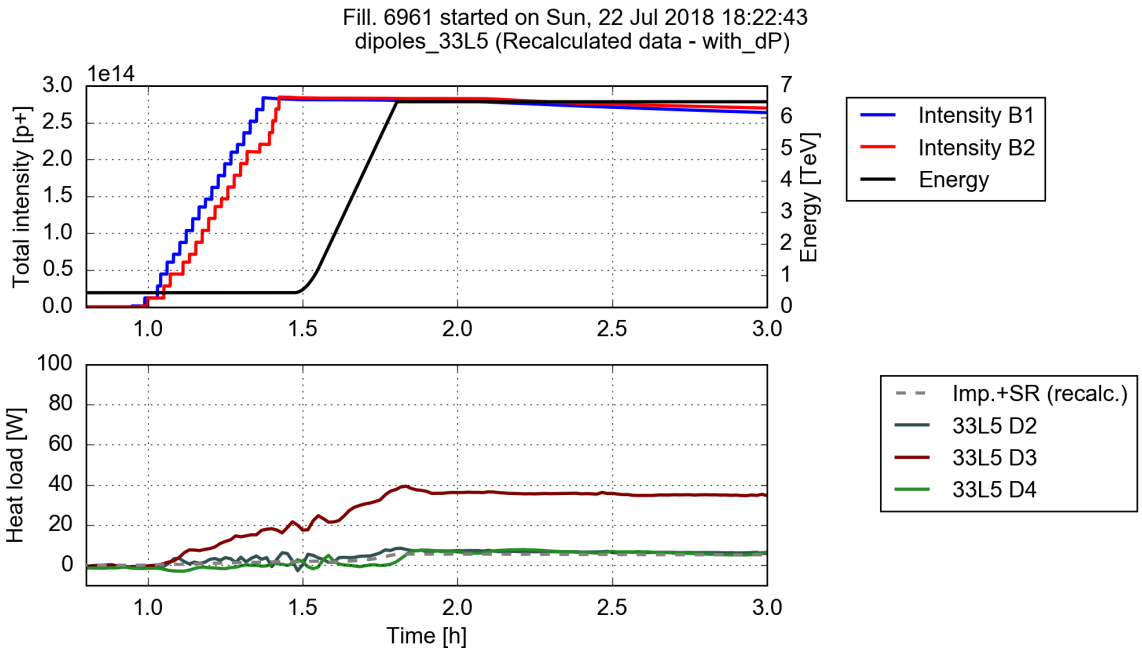

Figure 12: Heat loads on the beam screens of the instrumented dipoles in the half-cell 33L5.

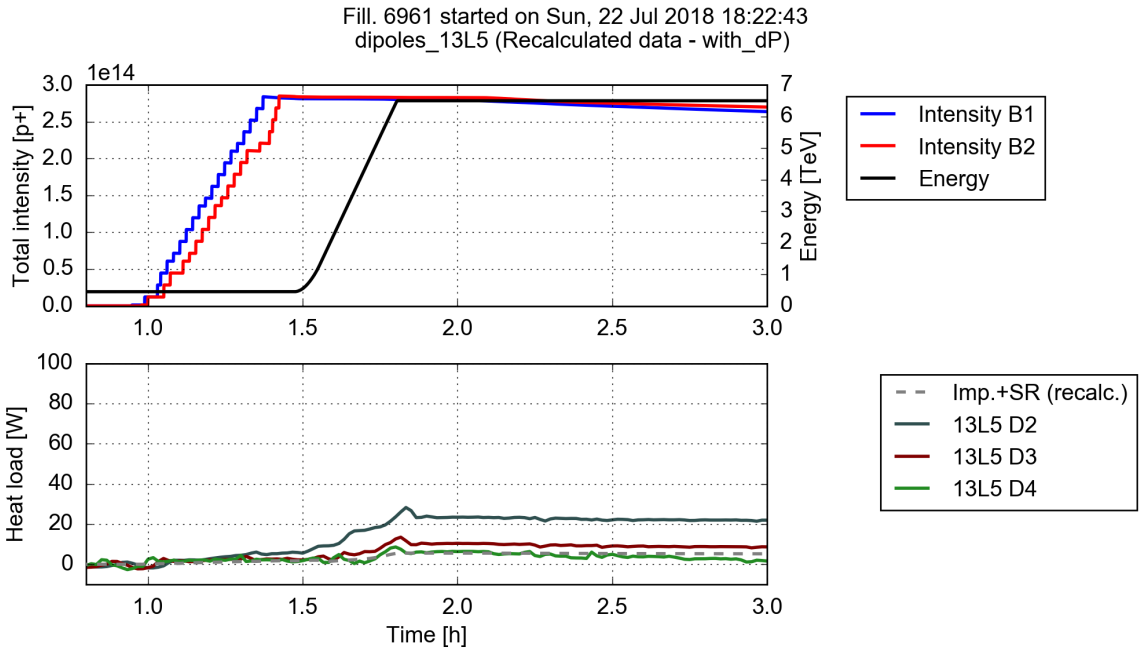

Figure 13: Heat loads on the beam screens of the instrumented dipoles in the half-cell 13L5.

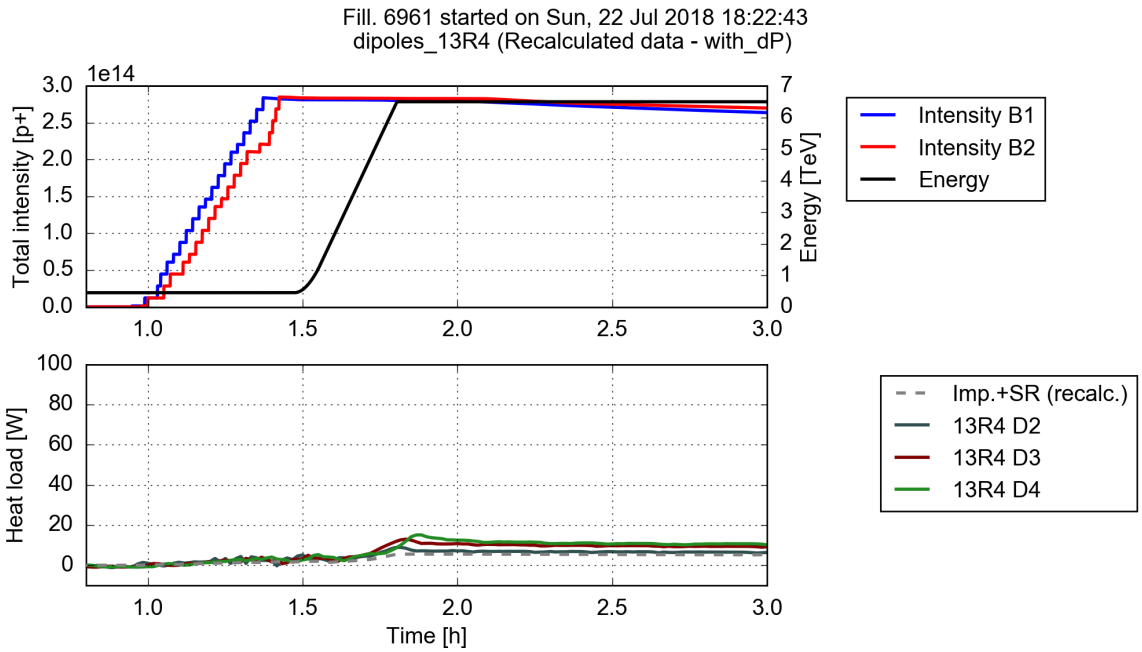

Figure 14: Heat loads on the beam screens of the instrumented dipoles in the half-cell 13R4.

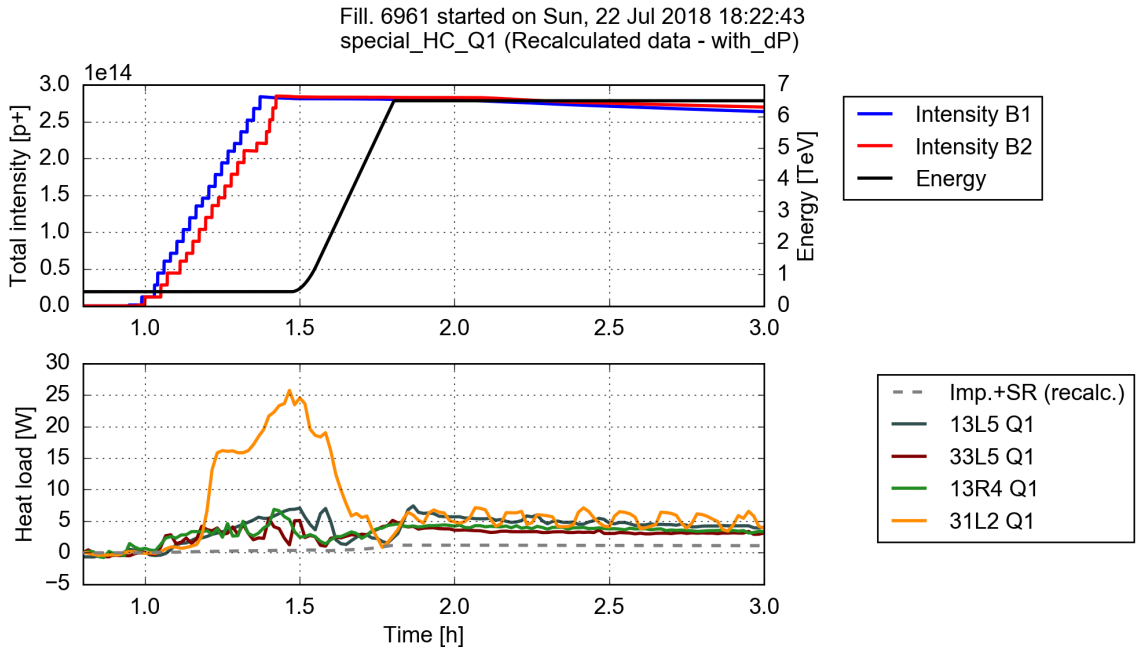

Figure 15: Heat loads on the beams screens of the instrumented quadrupoles in the half-cells 31L2, 33L5, 13L5 and 13R4.

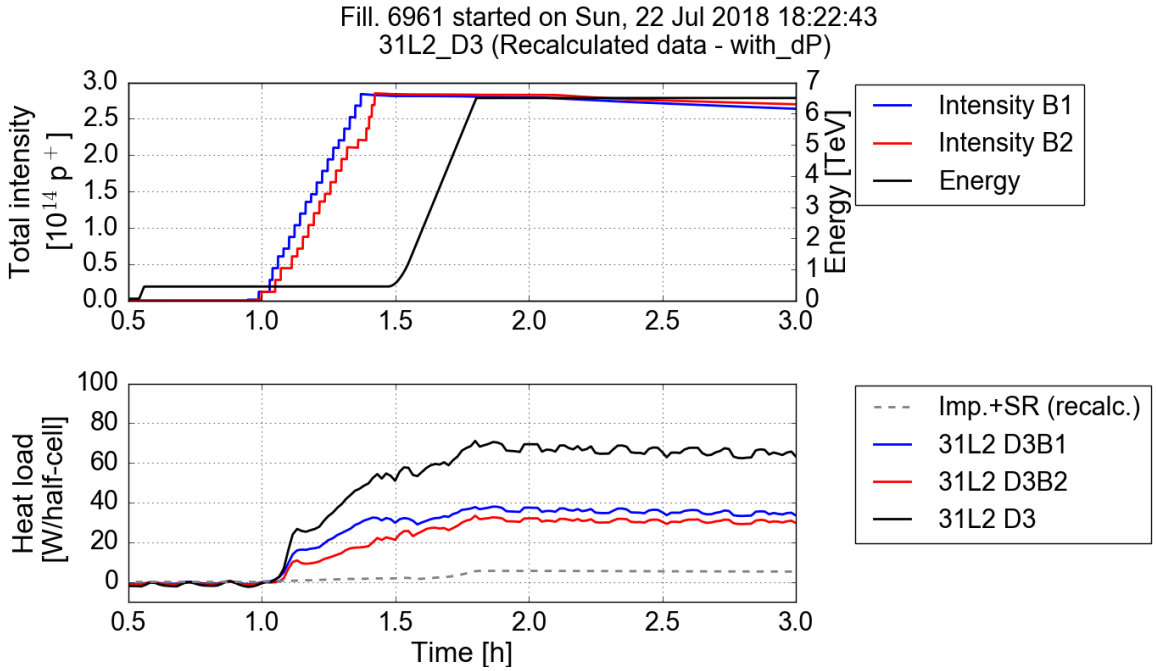

Figure 16: Heat loads on the two apertures for the instrumented dipole D3 in the half-cell 31L2.

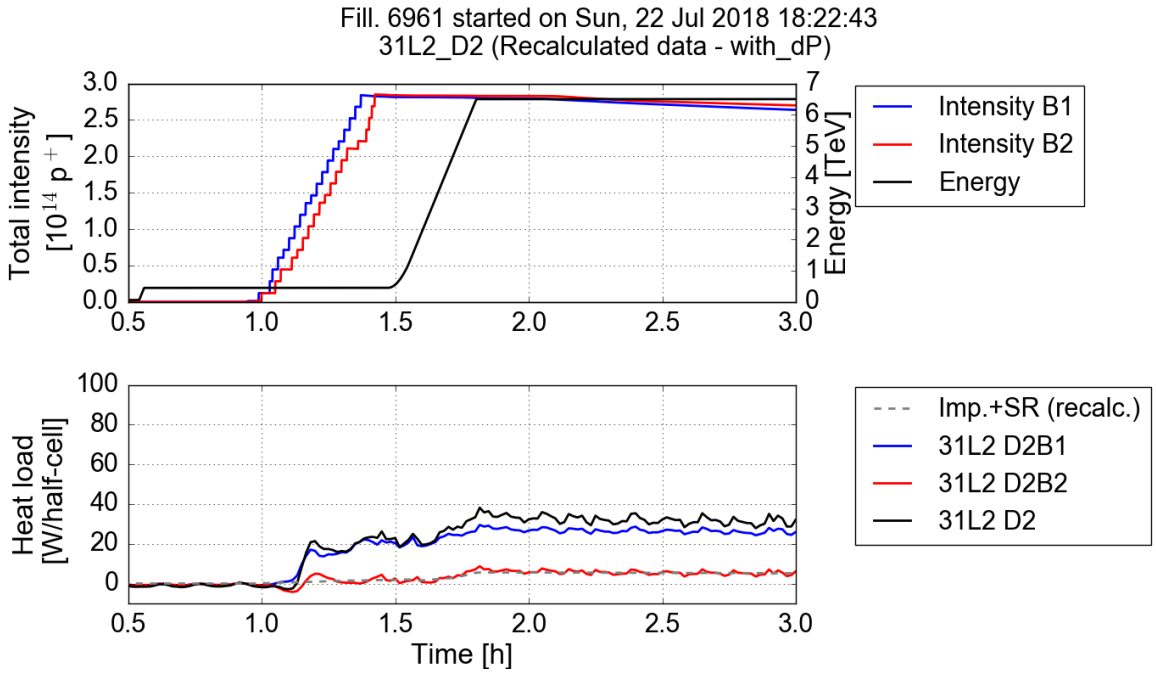

Figure 17: Heat loads on the two apertures for the instrumented dipole D2 in the half-cell 31L2.

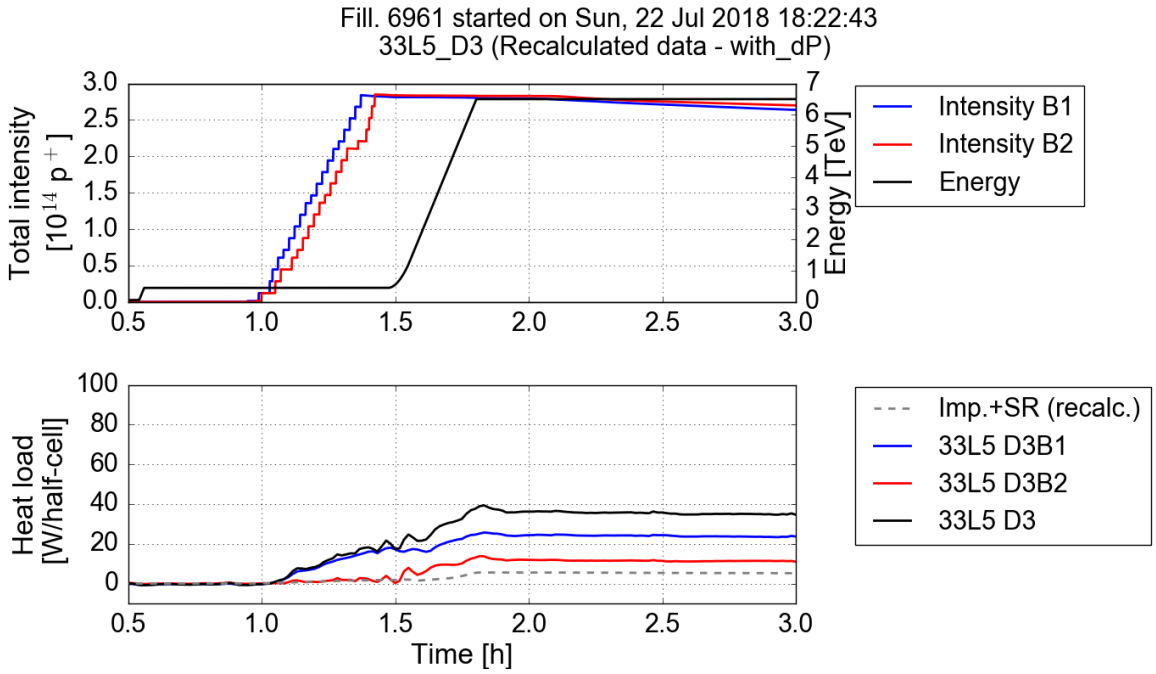

Figure 18: Heat loads on the two apertures for the instrumented dipole D3 in the half-cell 33L5.

2.2 Dependence on the number of circulating bunches

In order to assess the dependence of the heat loads on the number of circulating bunches, data were collected from fills performed at 450 GeV with different number of bunches. The measured heat loads are showed in Fig. 19. All measurements were taken with filling schemes using injections of 4×48 bunches, and keeping the bunch intensity and all other machine and beam parameters equal to the 2018 operational values.

Figure 19 shows that the dependence of the heat loads on the number of circulating bunches is practically linear for all arcs.

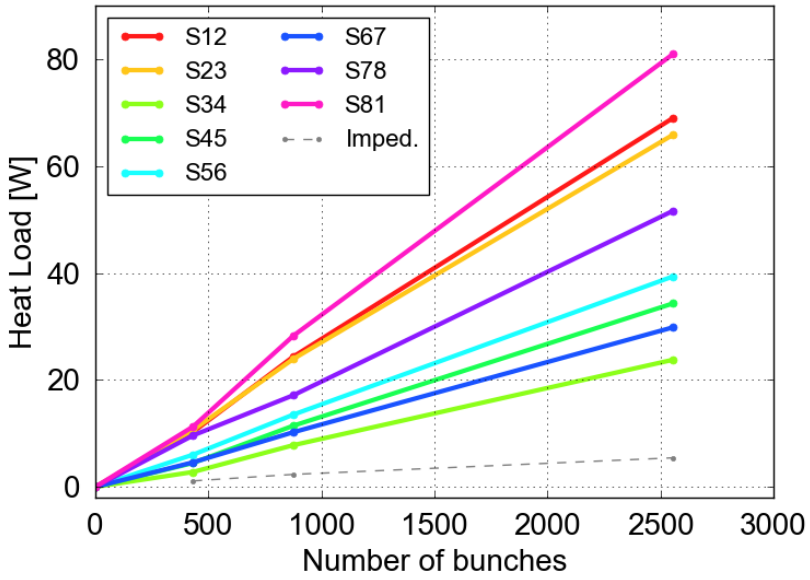

Figure 19: Average heat load per half-cell measured in fills with different number of bunches (fill 6786 (2556b), fill 6788 (876b), fill 7161 (432b)).

2.3 Dependence on the bunch intensity

In view of the planned HL-LHC project [3], which foresees a twofold increase of the beam intensity, it is of particular interest to study the dependence of the heat loads on the bunch population.

This was done in different MD sessions labelled as MD3300 in Tab. 1. The test consisted in five fills performed at 450 GeV with different bunch populations in the range 0.3 - 1.2 $\times 10^{11}$ p/bunch, using trains of 3×48 bunches. The filling pattern and all other machine and beam parameters were kept equal to the 2018 operational values. For the lower values of the bunch intensity, the settings of the transverse feedback needed to be adjusted.

The heat loads measured in the eight arcs during this test are shown in Fig. 20 (top). The expected contribution from impedance and synchrotron radiation is subtracted from the measured values. The measurements show that the heating from e-cloud becomes significant only above a certain threshold bunch intensity close to 0.4 $\times 10^{11}$ p/bunch. This behaviour is

expected for the e-cloud formation in the LHC main magnets [8] and was already observed experimentally at the SPS, with direct e-cloud measurements through strip detectors (in particular for MBA type chambers having the same height as the LHC beam screens) [9].

Figure 21 shows the heat loads recorded during the same experiment on the beam screens of selected instrumented arc magnets. The expected contribution from impedance and synchrotron radiation is subtracted from the measured values. In the dipole magnets (top plot) in which a significant heat load can be detected, a threshold effect around 0.4×10^{11} p/bunch can be observed, similar to the arc average heat loads. For the quadrupole magnets (bottom plot) the threshold is higher.

Direct heat load measurements above 1.2×10^{11} p/bunch were not possible in Run 2 using long bunch trains due to intensity limitations in the injectors (mainly RF power limitations in the SPS [10, 11]). Towards the end of 2018, trains of 12 bunches with high bunch intensity, up to 1.9×10^{11} p/bunch, became available from the SPS and were used for tests in the LHC during the last MD block with protons, in the MD4203 session.

The test consisted of four consecutive fills with different bunch intensity, using a filling scheme with 1020 bunches per beam, made of injections of 4×12 bunches. The evolution of the beam intensity and of the arc heat loads during the test is illustrated in Fig. 22. During the test, the settings of the transverse feedback needed to be adjusted in order to cope with the higher bunch intensity. The cryogenics feed-forward regulations were disabled during these measurements.

More than four hours in the beginning of the MD session were required to prepare the injection of bunch trains with high bunch intensity. In particular, it was necessary to carefully optimize the RF settings in the SPS to mitigate longitudinal instabilities and achieve an acceptable beam quality. However, even with the best configuration that could be found in the SPS, the beams were dumped several times at injection, due to losses caused by uncaptured beam and "satellite bunches" deflected by the injection kickers on the injection absorber (TDI). This was mitigated by systematically pulsing the injection kickers without incoming beam before each injection, in order to "clean" the portion of the ring in which the next bunch train was injected. The following fills with lower bunch intensities were not affected by these issues.

The heat loads measured in the eight arcs during the test are shown in Fig. 20 (bottom). The expected contribution from impedance and synchrotron radiation is subtracted from the measured values. The measurements show that above 1.5×10^{11} p/bunch the heat load produced by e-cloud tends to saturate and, for some arcs, even slightly decreases. This behaviour is expected from e-cloud buildup simulations and is discussed in detail in Sec. 3.

This test also provided interesting information from the point of view of beam stability. During the entire MD the chromaticity settings were $Q'_{x,y}$=15 for both beams. The beam with the highest bunch intensity was stable even without any current in the Landau octupoles. Instead, with bunch intensities lower than 0.75×10^{11} p/bunch, vertical instabilities were observed on the trailing bunches of the trains, even with octupole currents as large as 50 A [12]. This counter-intuitive behaviour of instabilities driven by e-cloud as a function of the bunch population was already observed at the LHC and is discussed in [13].

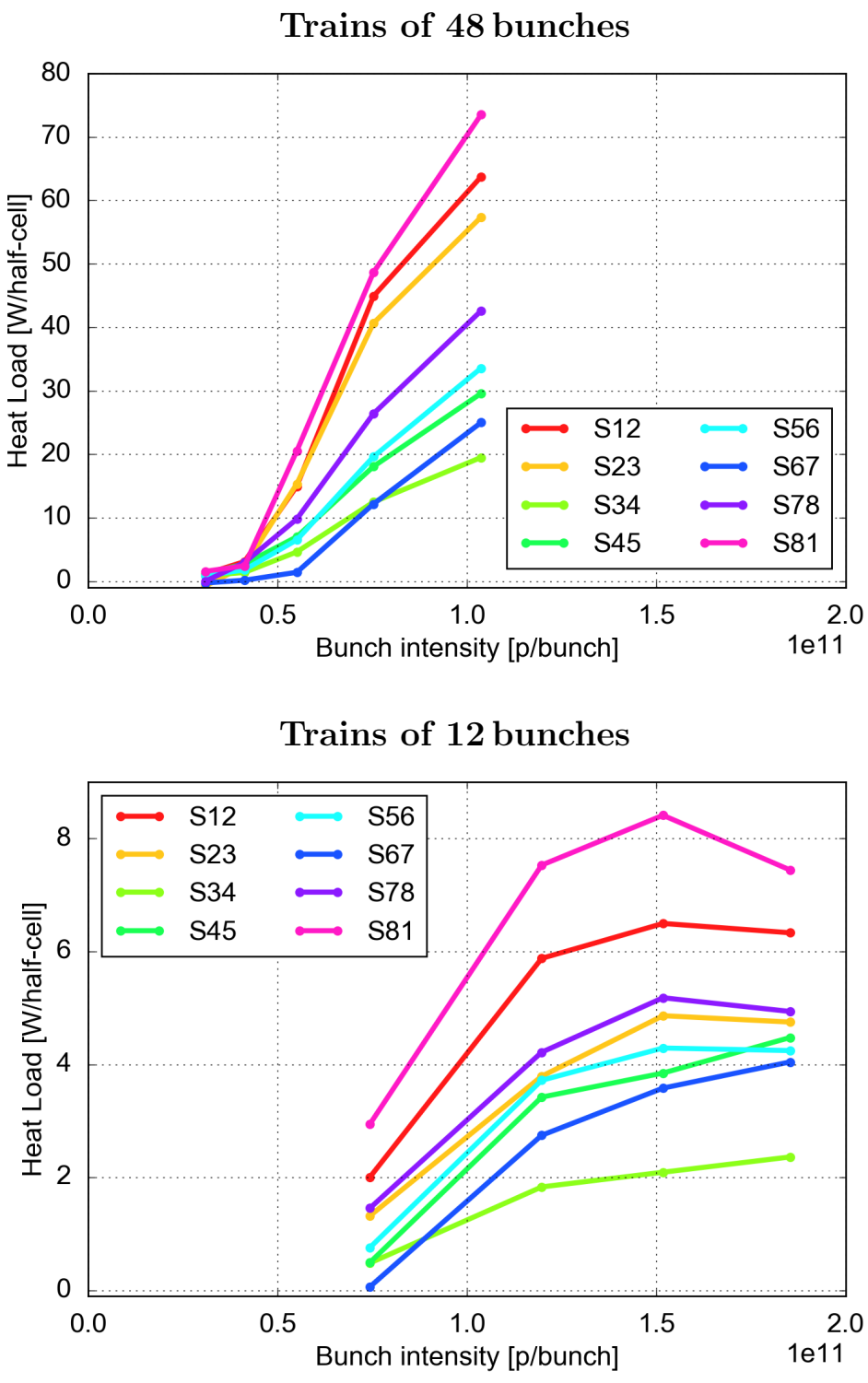

Figure 20: Heat loads measured at 450 GeV with different bunch populations with trains of 48 bunches (top) and with trains of 12 bunches (bottom). In the plots the contributions from impedance and synchrotron radiation are subtracted.

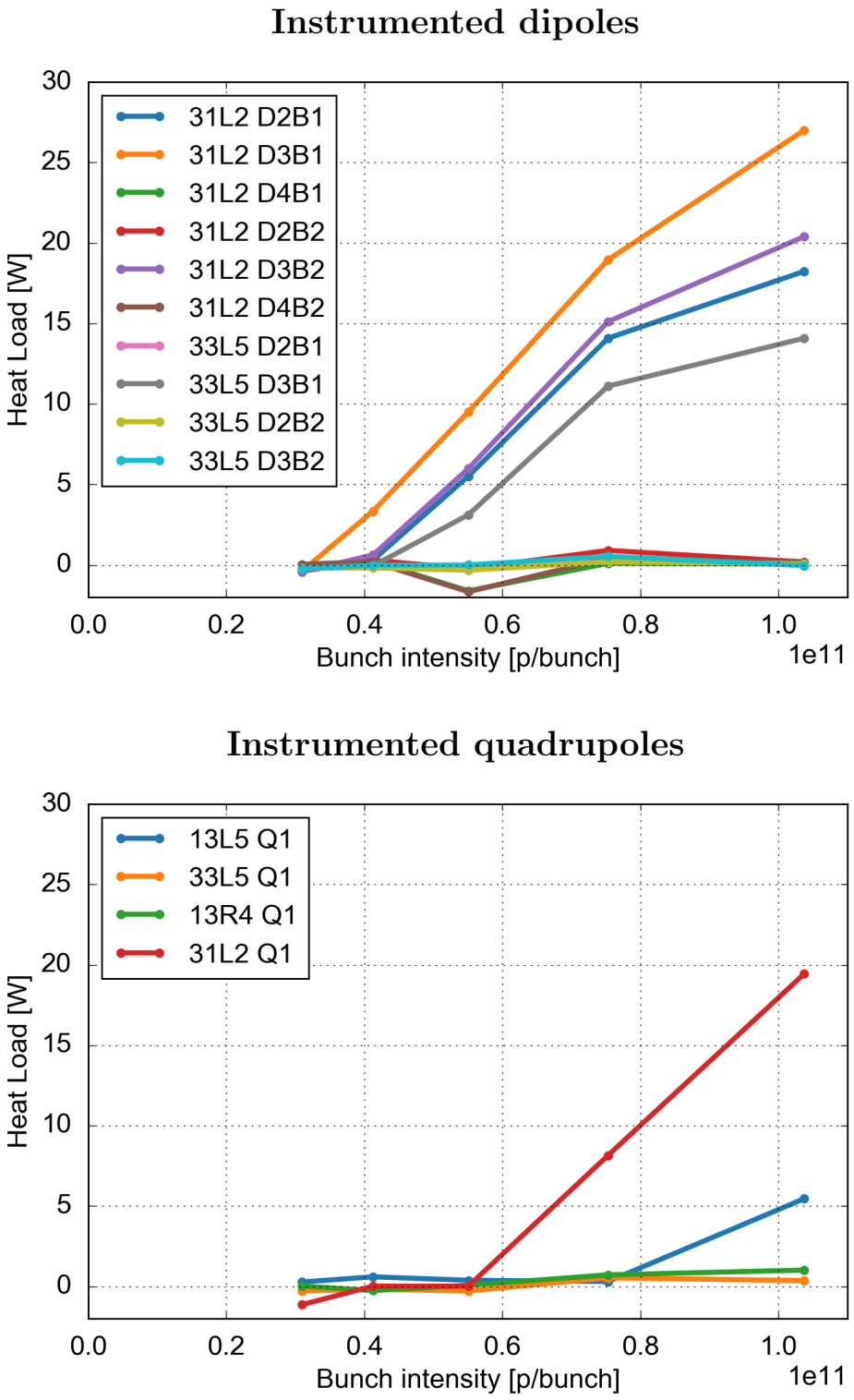

Figure 21: Heat loads measured at 450 GeV in the instrumented dipoles (top) and in the instrumented quadrupoles (bottom) with different bunch populations with trains of 48 bunches. In the plots the contributions from impedance and synchrotron radiation are subtracted.

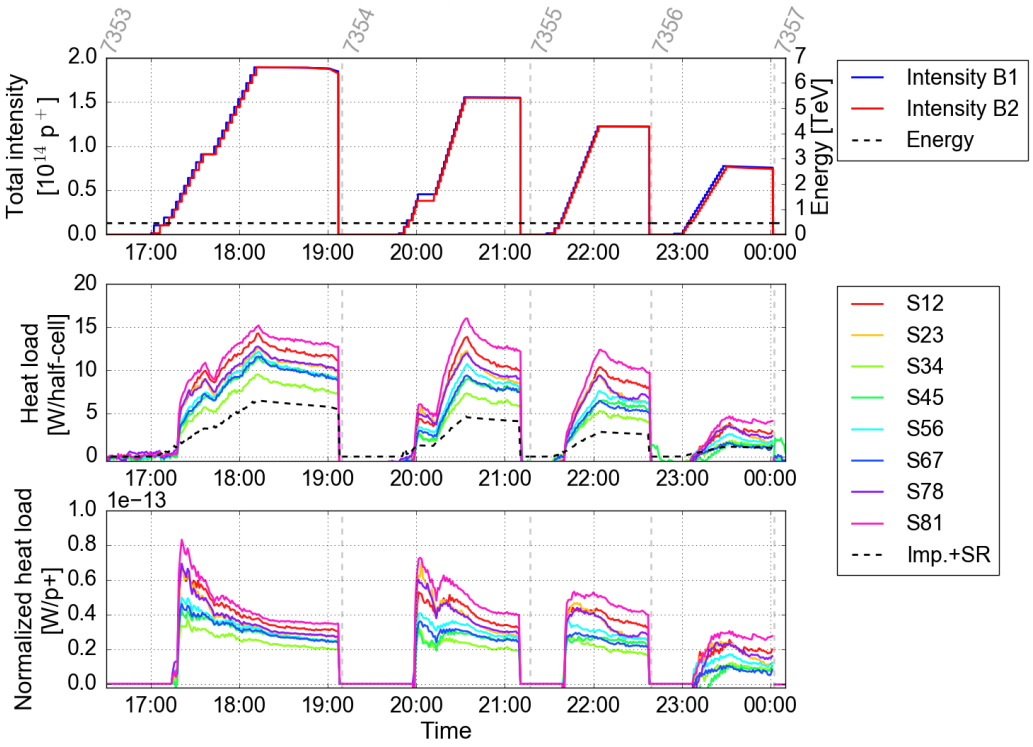

Figure 22: Evolution of the beam intensities and of the arc heat loads during the MD4203 session.

2.4 Dependence on the bunch length

In order to better characterize the source of the beam-induced heat loads, the dependence on the bunch length was investigated in a dedicated test at injection energy during the MD3298 session.

Before performing the measurements, it was necessary to assess the bunch length range that could be reached with acceptable losses and abort-gap population. This was done in a preliminary fill with a reduced number of bunch trains. The minimum achieved bunch length was about 0.85 ns (four rms-sigmas). This was obtained by injecting the beam with 6 MV RF voltage, then switching to the full-detuning mode of the RF system and increasing the RF voltage to 15 MV. The maximum achieved bunch-length was about 1.6 ns and was obtained by reducing the RF voltage back to 6 MV and applying controlled longitudinal blow-up. All bunch length values quoted here are measured by the LHC Beam Quality Monitor, which measures the Full-Width at Half-Maximum and, from that, infers the r.m.s. bunch length assuming a Gaussian longitudinal profile.

A measurement fill was performed with 1020 bunches per beam using a filling scheme similar to the luminosity production one, with injections of 3×48 bunches and 25 ns bunch spacing. After the beam injection, the bunch length was reduced to about 0.85 ns and heat load data was collected for 15 minutes. After that, the bunch length was increased to 1.6 ns followed by 15 minutes of data collection.

It is particularly interesting to observe the effect of the bunch length on the individual magnets in the instrumented cells, as illustrated in Fig. 23. The dipole magnets in which a heat load is detectable, show a reduction of the heat load when the bunch length is

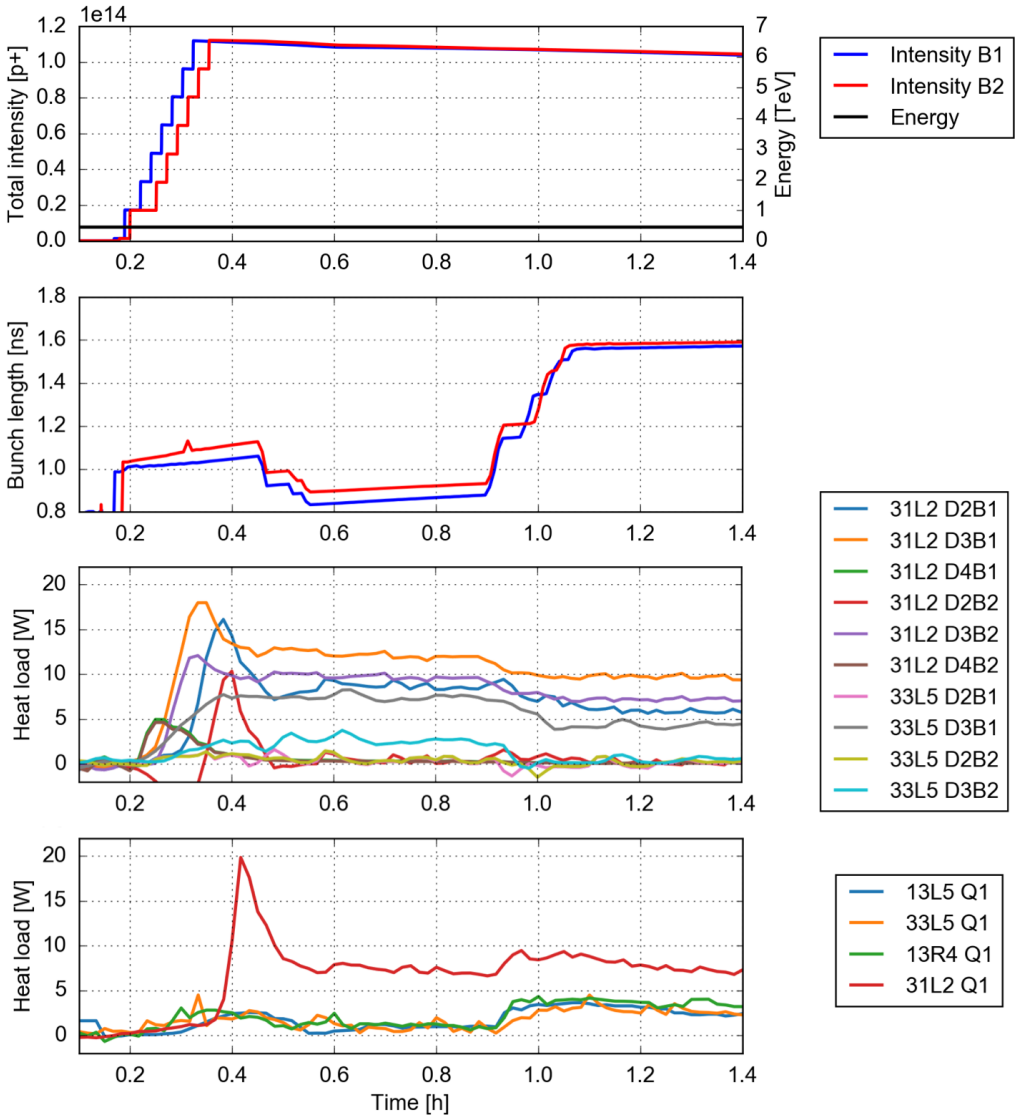

Figure 23: Heat load behaviour in the instrumented magnets during the MD 3298.

increased. The quadrupole magnets, instead, show the opposite behaviour with the heat load increasing when the bunch length is increased. Such different behaviour for dipole and quadrupole magnets is expected for e-cloud effects [14]. It is instead incompatible with other heating mechanisms, and in particular with impedance heating, for which the magnetic field configuration should have no impact on its behaviour as a function of the bunch length.

Figure 24 shows the evolution of the average heat load in the eight arcs during the experiment. In all arcs a reduction of the heat load is observed when increasing the bunch length. This indicates that the total heat load is dominated by the contribution of the dipoles.

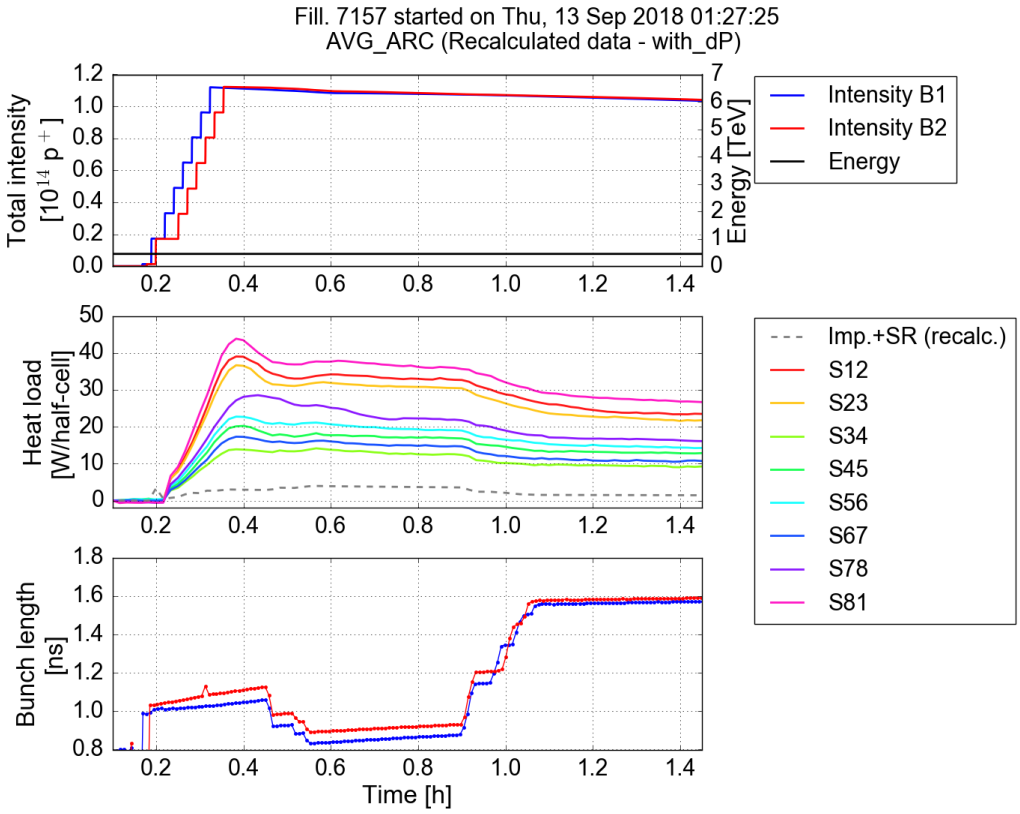

Figure 24: Heat load behaviour in the LHC arcs during the MD 3298.

2.5 Test with high-intensity 8b+4e beams

The 8b+4e scheme is a bunch pattern made of short trains of eight bunches separated by gaps of four empty slots. Based on numerical simulations, such a pattern is expected to significantly mitigate the e-cloud formation for bunch intensities up to the HL-LHC target [8].

For the nominal bunch intensity, the e-cloud reduction has been proved experimentally in the LHC in 2015 [15] and this scheme was used for luminosity production in the second part of the 2017 run, to mitigate issues related to an accidental air release into the beam pipe in the arc cell 16L2 [16]. In 2018, 8b+4e beams with higher bunch intensity became available from the injectors and were tested in the LHC during the MD2484 session.

Two fills were performed with 8b+4e beams with bunch intensity close to 1.55×10^{11} p/bunch, as illustrated in Fig. 25, the first with 852 bunches and the second with 1812 bunches. When injecting the first fill, the beam was dumped a few times on losses right at injection (for Beam 1), probably due to showers from the TCDI transfer-line collimator. This was mitigated by increasing the transverse scraping in the SPS and optimizing the trajectory in the transfer line. The settings of the transverse feedback had to be optimized to operate with higher bunch intensity. The cryogenics feed-forward regulations were disabled during the test.

It was originally planned to perform both fills using a special optics with a large telescopic factor and $\beta^* = 65\,\text{cm}$, which had been developed and tested in previous MD sessions [17].

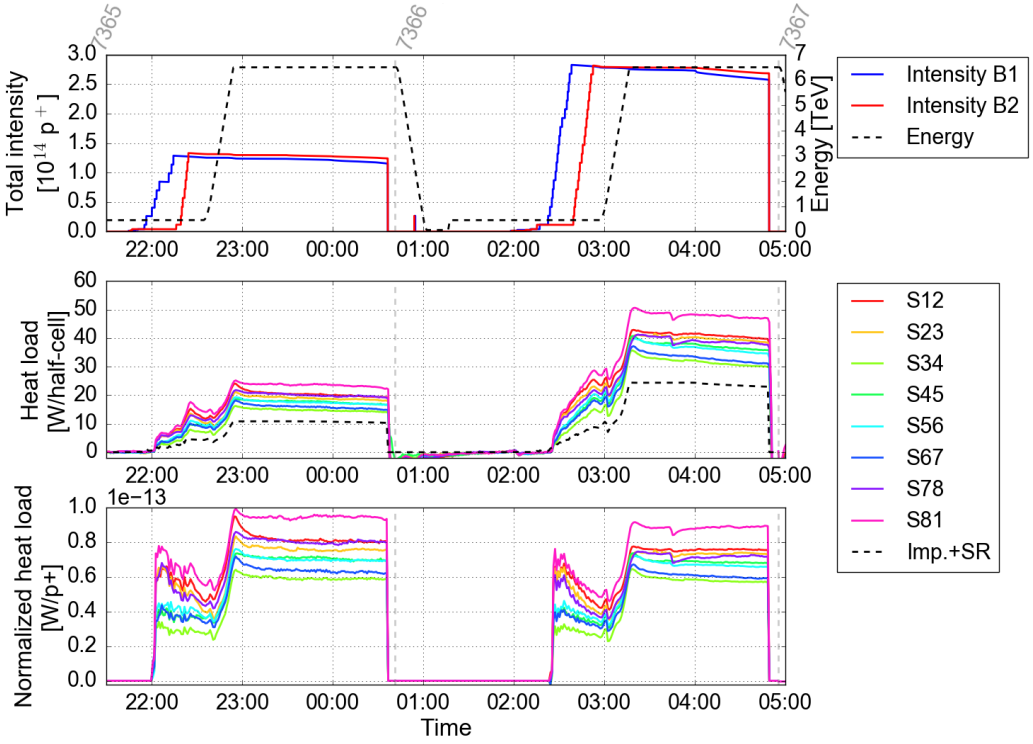

Figure 25: Evolution of the beam intensity and the heat loads during the MD2484 session.

This was employed only for the first fill, since it was noticed that the losses on the tertiary collimators would have been incompatible with the set dump threshold, when scaled to the full number of bunches. For this reason, it was decided to perform the second fill using the operational configuration with smaller telescopic factor and $\beta^* = 30\,\text{cm}$.

The heat loads measured in the eight arcs during the tests never exceeded by more than 30 W/half-cell the value expected from impedance and synchrotron radiation, as shown in Fig. 25.

In Fig. 26, the heat loads measured at high energy with 8b+4e beams having 1.5×10^{11} p/bunch (in green) are compared against those measured with standard 25 ns beams with nominal intensity, (1.1×10^{11} p/bunch in blue) and 8b+4e beams with nominal intensity (1.1×10^{11} p/bunch, in red). The large suppression of the heat loads due to e-cloud is evident. The heat load increase observed with 8b+4e beams when increasing the bunch intensity from 1.1×10^{11} p/bunch to 1.5×10^{11} p/bunch is found to be very modest. Similar features are observed at a cell-by-cell level as shown in Figs. 27 - 30. This result contributes to the validation of the 8b+4e scheme as a backup scenario for the HL-LHC project, in case limitations from e-cloud would prevent utilizing the design bunch pattern.

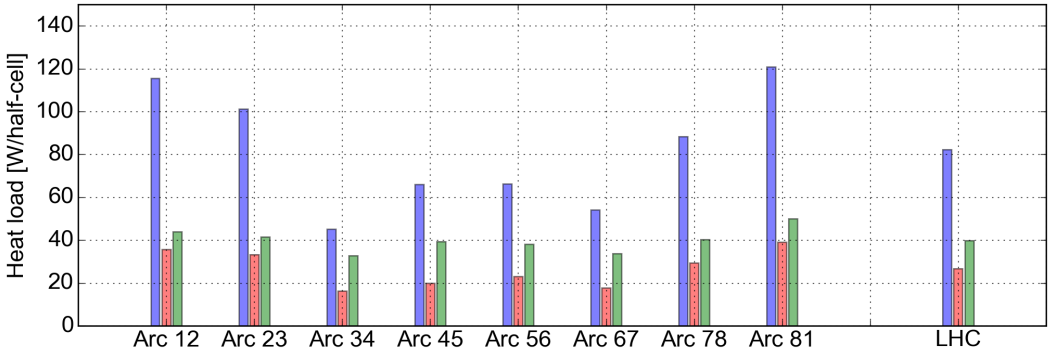

Fill	6961	6243	7366
Started on	22 Jul 2018 18:22	25 Sep 2017 18:49	27 Oct 2018 00:41
T_sample [h]	2.00	2.50	3.30
Energy [GeV]	6499	6499	6499
N_bunches (B1/B2)	2556/2556	1916/1916	1812/1812
Intensity (B1/B2) [p]	2.79e14/2.83e14	2.13e14/2.16e14	2.73e14/2.78e14
Bun.len. (B1/B2) [ns]	1.11/1.10	1.07/1.07	1.05/1.06
H.L. exp. imped. [W]	8.77	7.14	12.65
H.L. exp. synrad [W]	11.96	9.14	11.72
H.L. exp. imp.+SR [W/p+]	3.69e-14	3.79e-14	4.42e-14
T_nobeam [h]	0.90	0.20	1.00

Figure 26: Average heat loads measured in the LHC arcs with the standard 25 ns beam (blue), the 8b+4e beam with 1.1×10^{11} p/bunch (red) and the 8b+4e beam with 1.5×10^{11} p/bunch (green). The contributions from impedance and synchrotron radiation are subtracted from the plotted heat loads.

Arc 12

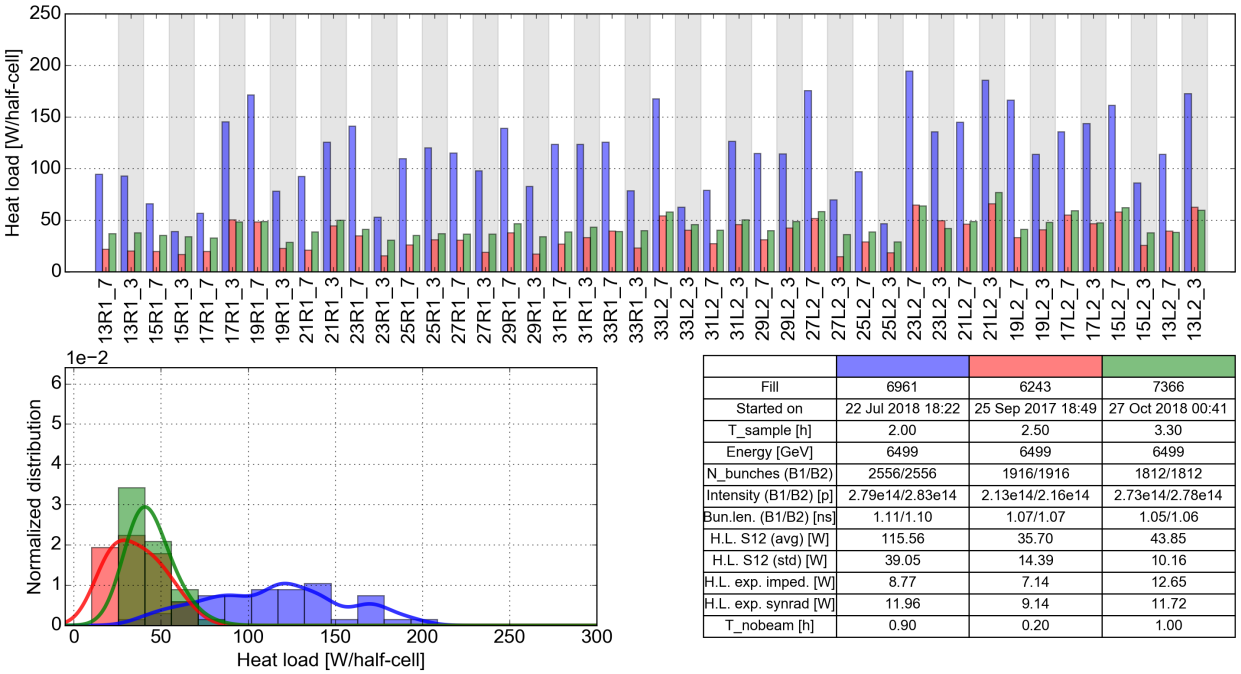

Fill	6961	6243	7366
Started on	22 Jul 2018 18:22	25 Sep 2017 18:49	27 Oct 2018 00:41
T_sample [h]	2.00	2.50	3.30
Energy [GeV]	6499	6499	6499
N_bunches (B1/B2)	2556/2556	1916/1916	1812/1812
Intensity (B1/B2) [p]	2.79e14/2.83e14	2.13e14/2.16e14	2.73e14/2.78e14
Bun.len. (B1/B2) [ns]	1.11/1.10	1.07/1.07	1.05/1.06
H.L. S12 (avg) [W]	115.56	35.70	43.85
H.L. S12 (std) [W]	39.05	14.39	10.16
H.L. exp. imped. [W]	8.77	7.14	12.65
H.L. exp. synrad [W]	11.96	9.14	11.72
T_nobeam [h]	0.90	0.20	1.00

Arc 23

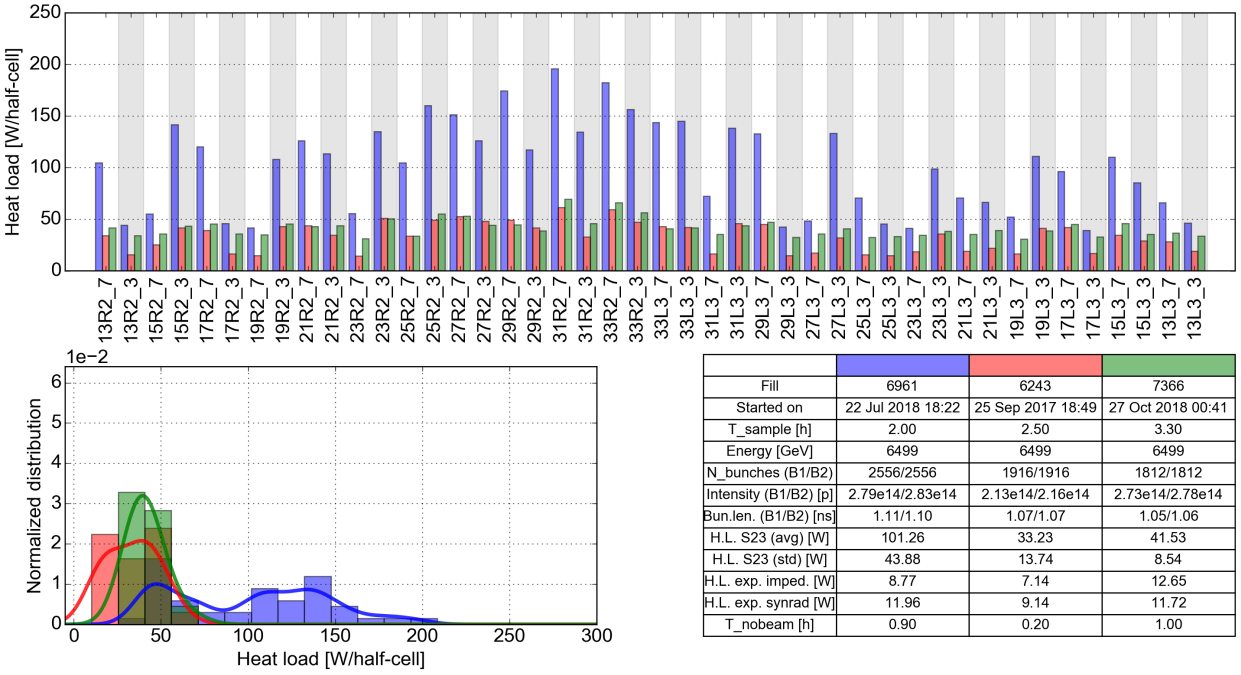

Fill	6961	6243	7366
Started on	22 Jul 2018 18:22	25 Sep 2017 18:49	27 Oct 2018 00:41
T_sample [h]	2.00	2.50	3.30
Energy [GeV]	6499	6499	6499
N_bunches (B1/B2)	2556/2556	1916/1916	1812/1812
Intensity (B1/B2) [p]	2.79e14/2.83e14	2.13e14/2.16e14	2.73e14/2.78e14
Bun.len. (B1/B2) [ns]	1.11/1.10	1.07/1.07	1.05/1.06
H.L. S23 (avg) [W]	101.26	33.23	41.53
H.L. S23 (std) [W]	43.88	13.74	8.54
H.L. exp. imped. [W]	8.77	7.14	12.65
H.L. exp. synrad [W]	11.96	9.14	11.72
T_nobeam [h]	0.90	0.20	1.00

Figure 27: Cell-by-cell heat loads measured in the arc 12 and in the arc 23 with the standard 25 ns beam (blue), the 8b+4e beam with 1.1×10^{11} p/bunch (red) and the 8b+4e beam with 1.5×10^{11} p/bunch (green). The contributions from impedance and synchrotron radiation are subtracted from the plotted heat loads.

Arc 34

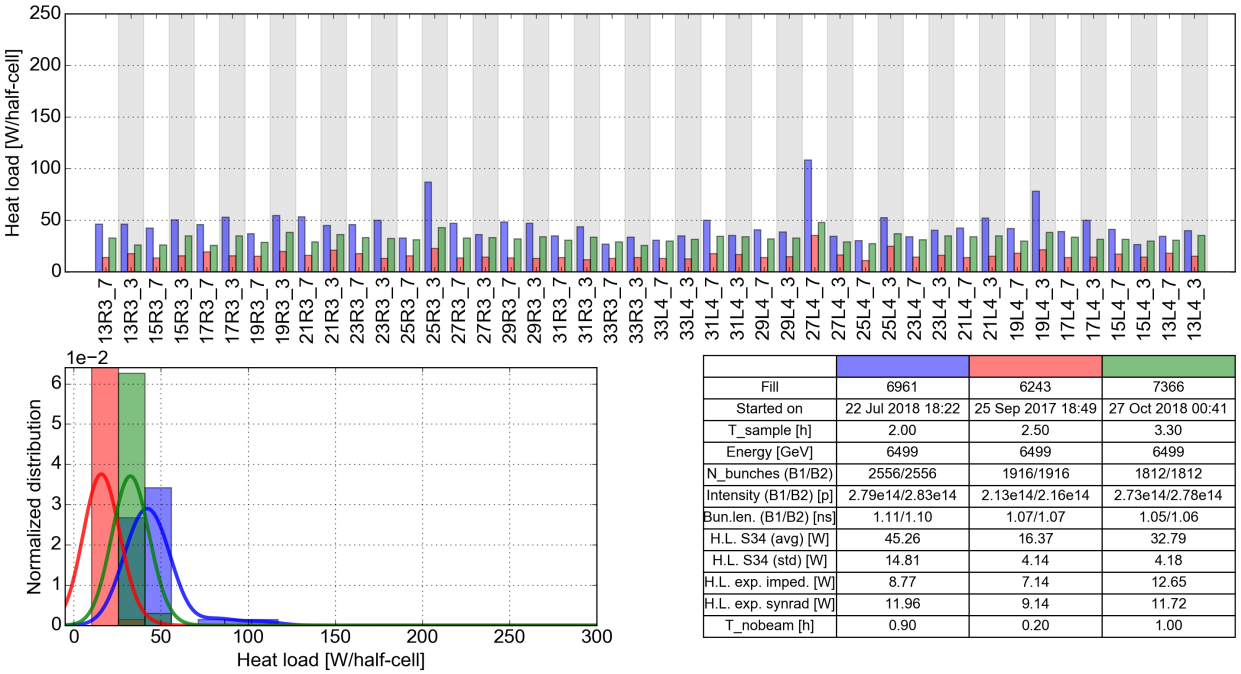

Fill	6961	6243	7366
Started on	22 Jul 2018 18:22	25 Sep 2017 18:49	27 Oct 2018 00:41
T_sample [h]	2.00	2.50	3.30
Energy [GeV]	6499	6499	6499
N_bunches (B1/B2)	2556/2556	1916/1916	1812/1812
Intensity (B1/B2) [p]	2.79e14/2.83e14	2.13e14/2.16e14	2.73e14/2.78e14
Bun.len. (B1/B2) [ns]	1.11/1.10	1.07/1.07	1.05/1.06
H.L. S34 (avg) [W]	45.26	16.37	32.79
H.L. S34 (std) [W]	14.81	4.14	4.18
H.L. exp. imped. [W]	8.77	7.14	12.65
H.L. exp. synrad [W]	11.96	9.14	11.72
T_nobeam [h]	0.90	0.20	1.00

Arc 45

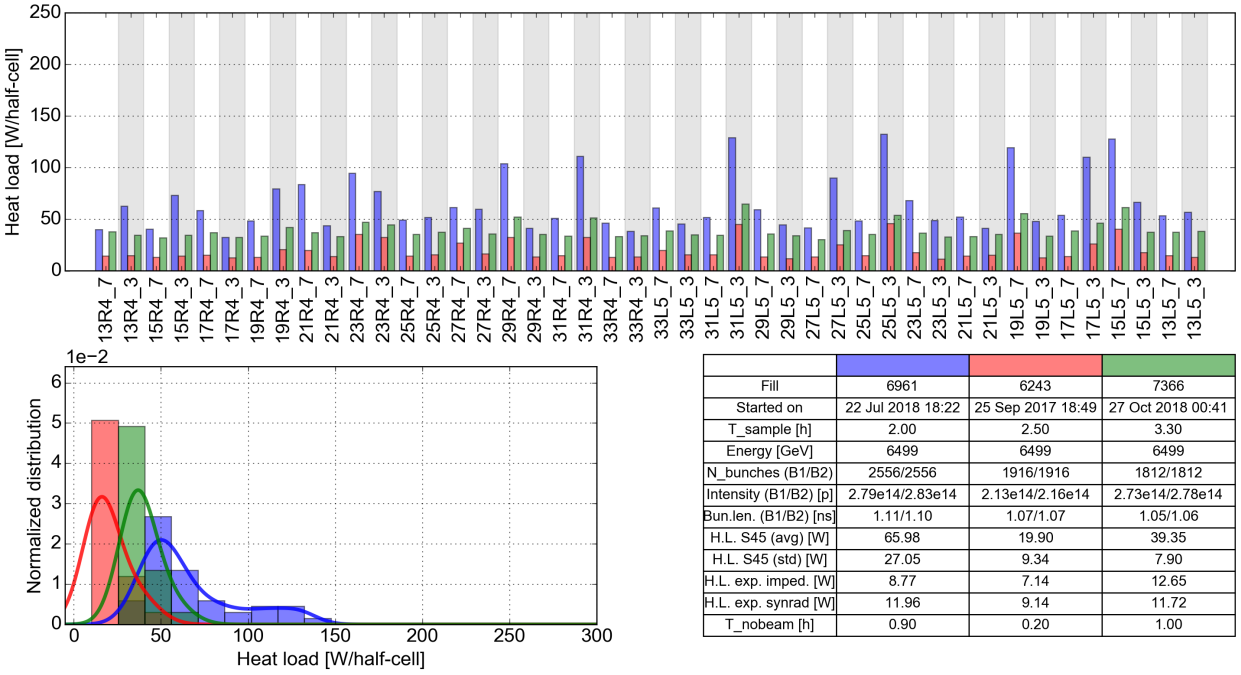

Fill	6961	6243	7366
Started on	22 Jul 2018 18:22	25 Sep 2017 18:49	27 Oct 2018 00:41
T_sample [h]	2.00	2.50	3.30
Energy [GeV]	6499	6499	6499
N_bunches (B1/B2)	2556/2556	1916/1916	1812/1812
Intensity (B1/B2) [p]	2.79e14/2.83e14	2.13e14/2.16e14	2.73e14/2.78e14
Bun.len. (B1/B2) [ns]	1.11/1.10	1.07/1.07	1.05/1.06
H.L. S45 (avg) [W]	65.98	19.90	39.35
H.L. S45 (std) [W]	27.05	9.34	7.90
H.L. exp. imped. [W]	8.77	7.14	12.65
H.L. exp. synrad [W]	11.96	9.14	11.72
T_nobeam [h]	0.90	0.20	1.00

Figure 28: Cell-by-cell heat loads measured in the arc 34 and in the arc 45 with the standard 25 ns beam (blue), the 8b+4e beam with 1.1×10^{11} p/bunch (red) and the 8b+4e beam with 1.5×10^{11} p/bunch (green). The contributions from impedance and synchrotron radiation are subtracted from the plotted heat loads.

Arc 56

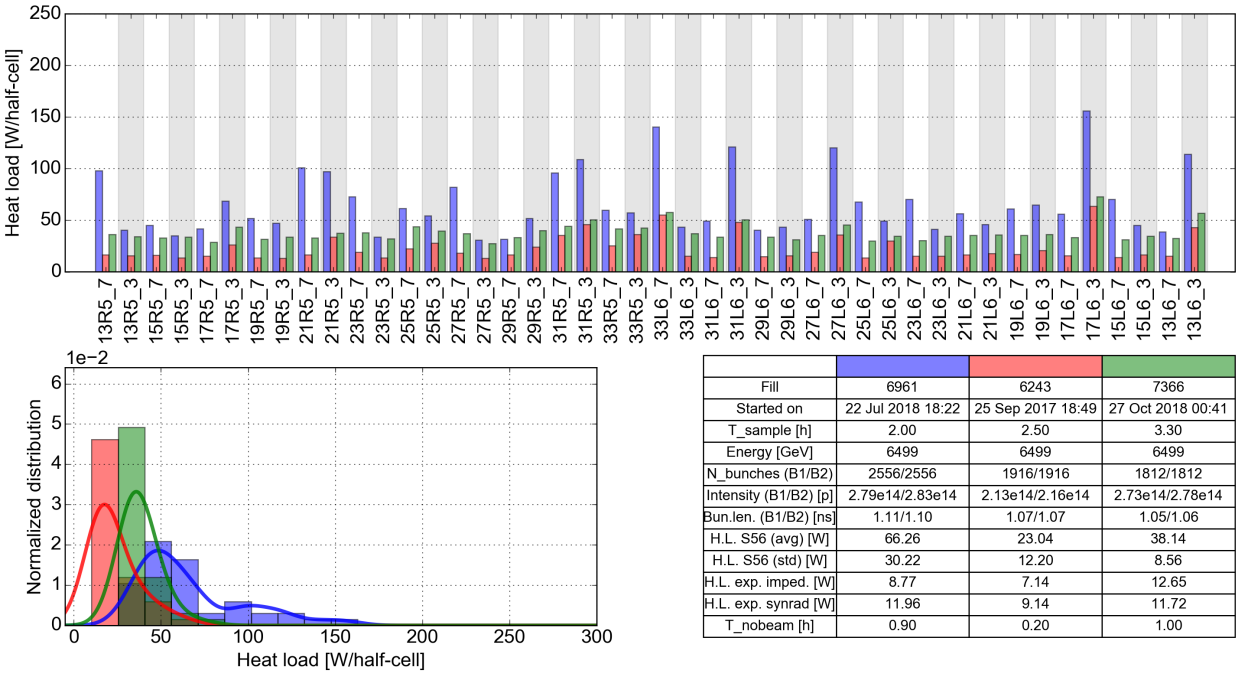

Fill	6961	6243	7366
Started on	22 Jul 2018 18:22	25 Sep 2017 18:49	27 Oct 2018 00:41
T_sample [h]	2.00	2.50	3.30
Energy [GeV]	6499	6499	6499
N_bunches (B1/B2)	2556/2556	1916/1916	1812/1812
Intensity (B1/B2) [p]	2.79e14/2.83e14	2.13e14/2.16e14	2.73e14/2.78e14
Bun.len. (B1/B2) [ns]	1.11/1.10	1.07/1.07	1.05/1.06
H.L. S56 (avg) [W]	66.26	23.04	38.14
H.L. S56 (std) [W]	30.22	12.20	8.56
H.L. exp. imped. [W]	8.77	7.14	12.65
H.L. exp. synrad [W]	11.96	9.14	11.72
T_nobeam [h]	0.90	0.20	1.00

Arc 67

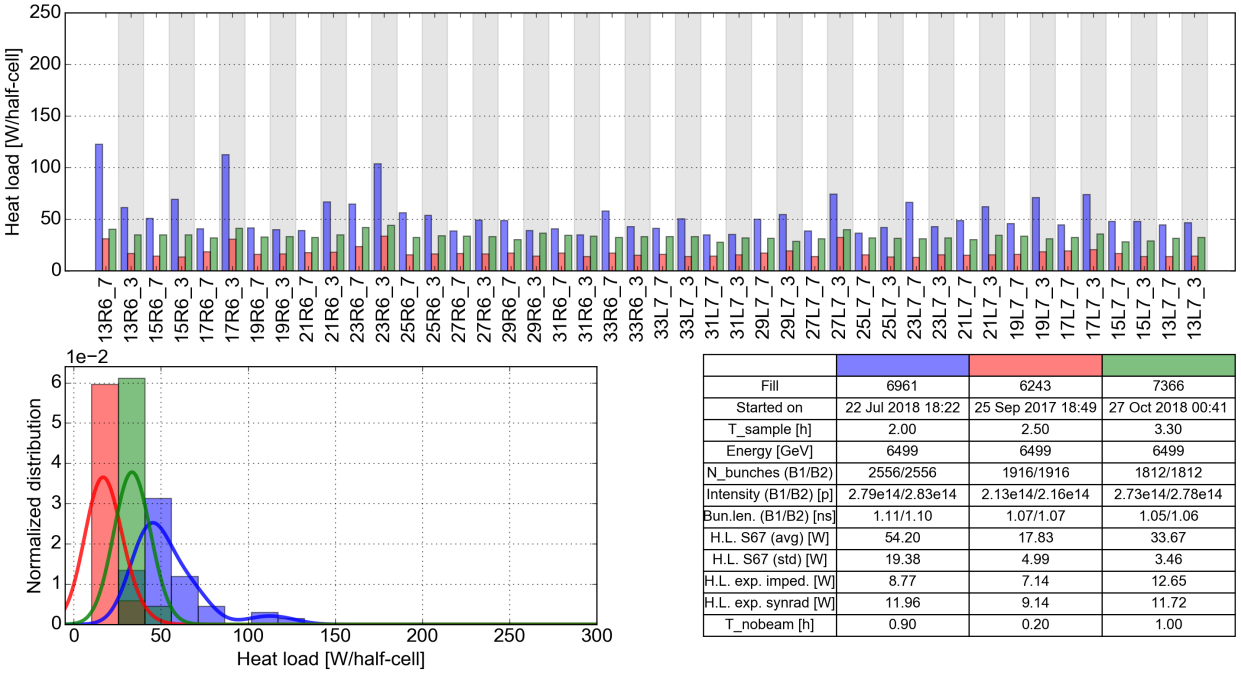

Fill	6961	6243	7366
Started on	22 Jul 2018 18:22	25 Sep 2017 18:49	27 Oct 2018 00:41
T_sample [h]	2.00	2.50	3.30
Energy [GeV]	6499	6499	6499
N_bunches (B1/B2)	2556/2556	1916/1916	1812/1812
Intensity (B1/B2) [p]	2.79e14/2.83e14	2.13e14/2.16e14	2.73e14/2.78e14
Bun.len. (B1/B2) [ns]	1.11/1.10	1.07/1.07	1.05/1.06
H.L. S67 (avg) [W]	54.20	17.83	33.67
H.L. S67 (std) [W]	19.38	4.99	3.46
H.L. exp. imped. [W]	8.77	7.14	12.65
H.L. exp. synrad [W]	11.96	9.14	11.72
T_nobeam [h]	0.90	0.20	1.00

Figure 29: Cell-by-cell heat loads measured in the arc 56 and in the arc 67 with the standard 25 ns beam (blue), the 8b+4e beam with 1.1×10^{11} p/bunch (red) and the 8b+4e beam with 1.5×10^{11} p/bunch (green). The contributions from impedance and synchrotron radiation are subtracted from the plotted heat loads.

Arc 78

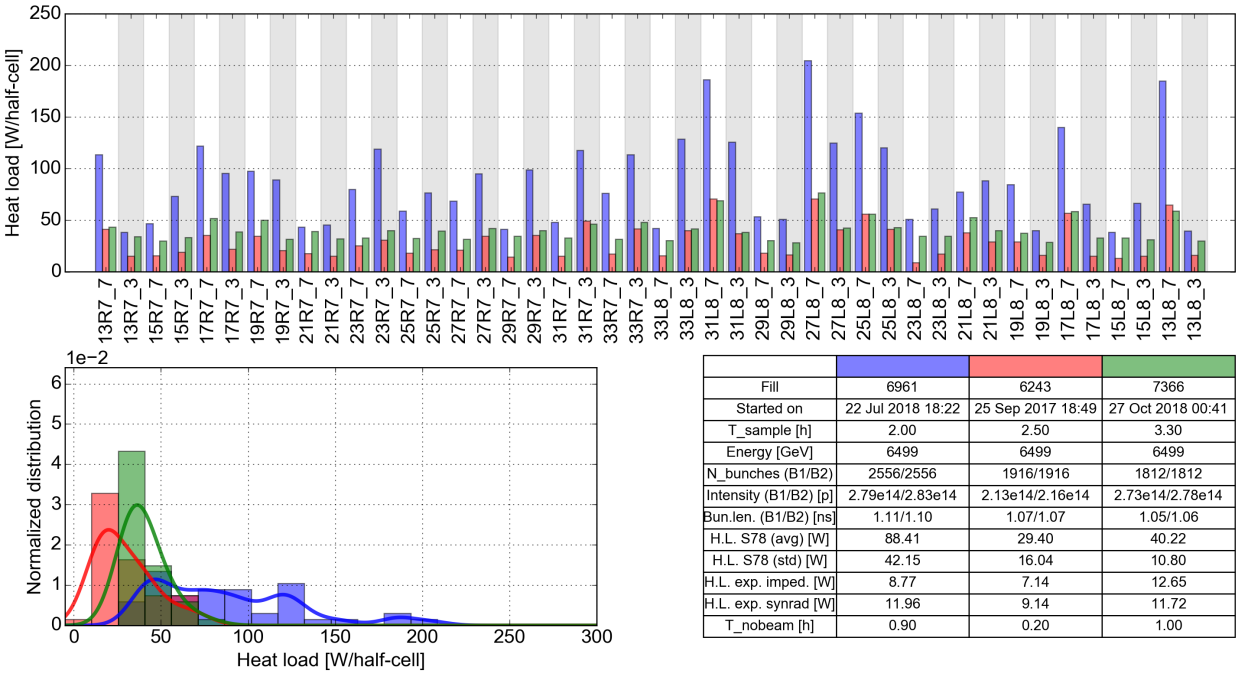

Fill	6961	6243	7366
Started on	22 Jul 2018 18:22	25 Sep 2017 18:49	27 Oct 2018 00:41
T_sample [h]	2.00	2.50	3.30
Energy [GeV]	6499	6499	6499
N_bunches (B1/B2)	2556/2556	1916/1916	1812/1812
Intensity (B1/B2) [p]	2.79e14/2.83e14	2.13e14/2.16e14	2.73e14/2.78e14
Bun.len. (B1/B2) [ns]	1.11/1.10	1.07/1.07	1.05/1.06
H.L. S78 (avg) [W]	88.41	29.40	40.22
H.L. S78 (std) [W]	42.15	16.04	10.80
H.L. exp. imped. [W]	8.77	7.14	12.65
H.L. exp. synrad [W]	11.96	9.14	11.72
T_nobeam [h]	0.90	0.20	1.00

Arc 81

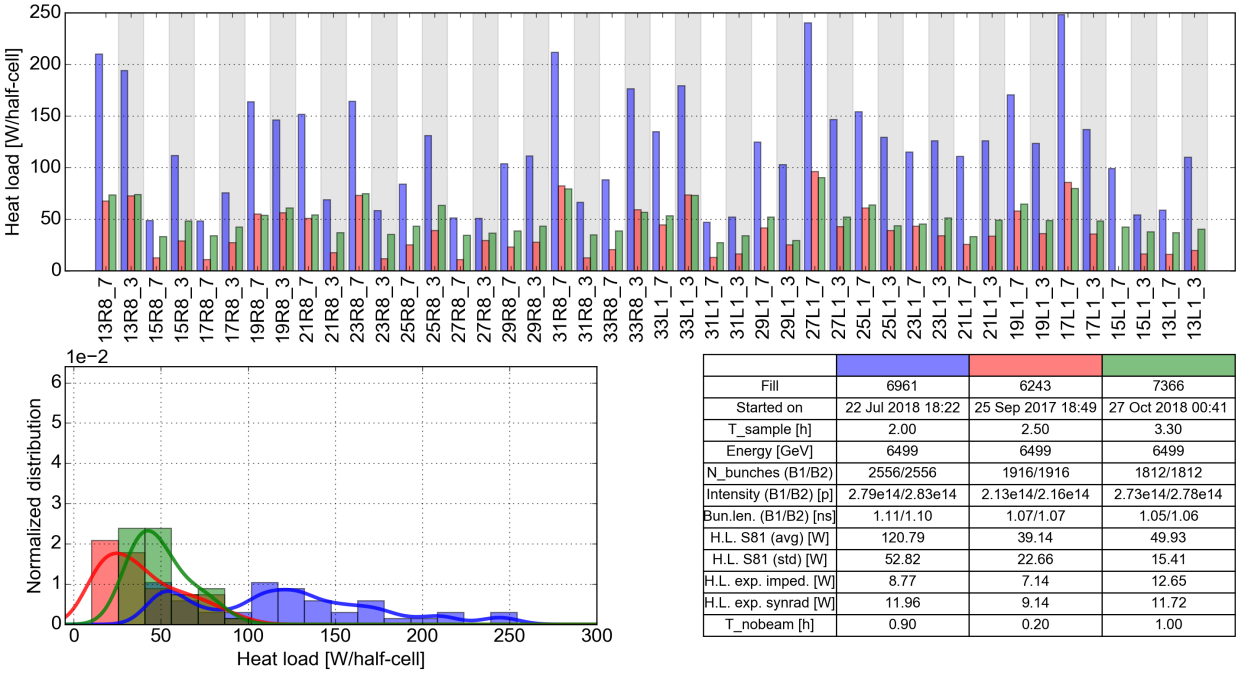

Fill	6961	6243	7366
Started on	22 Jul 2018 18:22	25 Sep 2017 18:49	27 Oct 2018 00:41
T_sample [h]	2.00	2.50	3.30
Energy [GeV]	6499	6499	6499
N_bunches (B1/B2)	2556/2556	1916/1916	1812/1812
Intensity (B1/B2) [p]	2.79e14/2.83e14	2.13e14/2.16e14	2.73e14/2.78e14
Bun.len. (B1/B2) [ns]	1.11/1.10	1.07/1.07	1.05/1.06
H.L. S81 (avg) [W]	120.79	39.14	49.93
H.L. S81 (std) [W]	52.82	22.66	15.41
H.L. exp. imped. [W]	8.77	7.14	12.65
H.L. exp. synrad [W]	11.96	9.14	11.72
T_nobeam [h]	0.90	0.20	1.00

Figure 30: Cell-by-cell heat loads measured in the arc 78 and in the arc 81 with the standard 25 ns beam (blue), the 8b+4e beam with 1.1×10^{11} p/bunch (red) and the 8b+4e beam with 1.5×10^{11} p/bunch (green). The contributions from impedance and synchrotron radiation are subtracted from the plotted heat loads.

2.6 Additional tests

This section describes two additional tests that were performed to assess the effects of the spool-piece correctors and closed-orbit distortions on the observed heat loads.

2.6.1 Effect of the field in the spool-piece correctors

In the MD3296 session a test was performed at injection energy to verify whether a significant fraction of the electrons is concentrated in the spool-piece correctors installed in each dipole.

Using pilot beams, the machine was configured to operate with the spool-piece correctors switched off in the arc 12 (one of the arcs showing higher heat load). In particular the B3 (sextupole) and B5 (decapole) corrections were redistributed on the other arcs (B4 corrections were already off as they are not used in operation). The test was made after several hours of operation at 450 GeV, so that no trim would be required from the FiDel model [18] to correct for the B3 and B5 decay (FiDel was paused during the entire experiment). These changes had no impact on the chromaticity, which confirms extremely good optics control. Due to feed-down effects a small change on the tunes was observed, which was corrected using the operational knobs, together with an increase of the linear coupling, which was corrected by optics specialists based on AC-dipole measurements.

In this machine configuration, with no field in the spool-piece correctors of the arc 12, the two LHC rings were filled with 2556 bunches and the heat load data was recorded for about 30 minutes. After that, with the beams still circulating in the two rings, the settings were reverted to the nominal ones and the heat loads were recorded for 30 more minutes.

In the following fill the same procedure was repeated switching off the spool-piece correctors in the arc 45 (one of the arcs showing lower heat load).

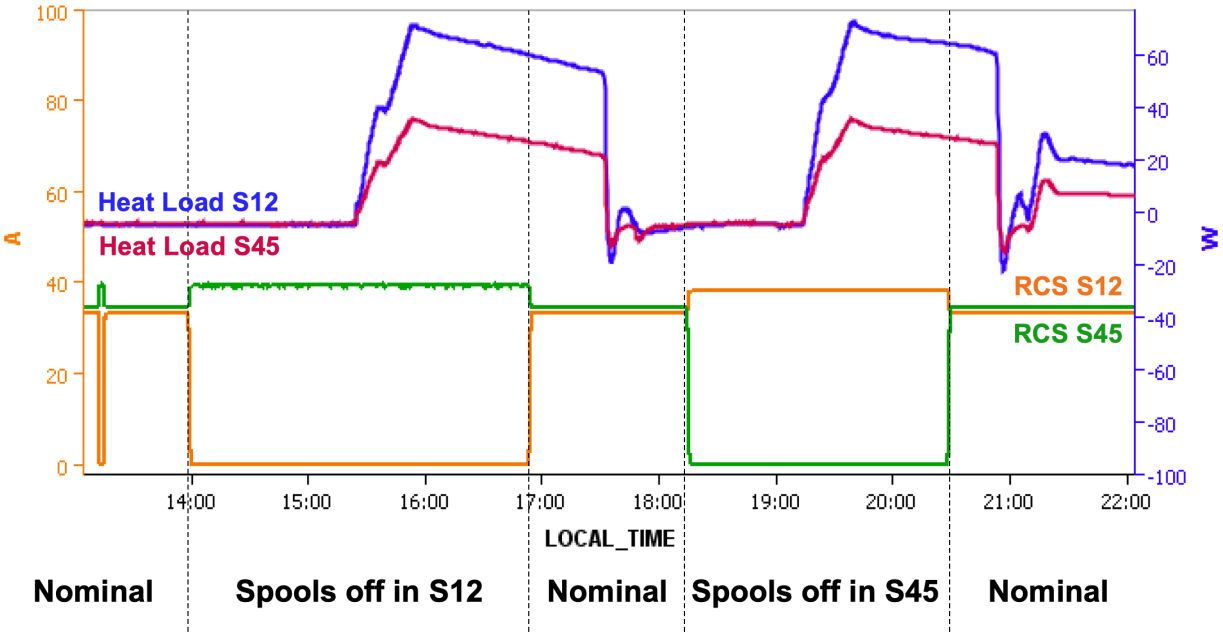

Figure 31: Current in the spool-piece sextupoles (RCS) and heat loads during the test.

Figure 31 shows the current in the spool-piece sextupoles and the heat loads for these two arcs during the experiment. It is evident that there is no visible effect of the field in the spool-piece correctors on the measured arc heat loads.

2.6.2 Effect of orbit bumps

The MD3297 session aimed at testing the sensitivity of the heat loads on changes of the closed orbit of the two beams.

For both beams, LSA knobs were created that introduced two orbit bumps in each of the LHC arcs. In each arc, one beam was displaced exclusively in the horizontal plane and the other beam was displaced exclusively in the vertical plane (to avoid exposing "skew" aperture bottlenecks). Table 2 shows the locations of the applied bumps, which include three of the specially instrumented cells discussed in Sec. 2.1.1. All the bumps use 4-correctors to distort the orbit in the shape shown in Figure 32. The peak distortion for all bumps was about 4 mm. Before applying the orbit distortion on high-intensity beams, the different machine configurations were validated by performing betatron and off-momentum loss maps and asynchronous dump tests.

For the heat load measurements, the two rings were filled with 876 bunches using the nominal closed orbit, then the orbit bumps were applied in all the selected cells and heat load data was collected in the following 15 minutes. After that, the sign of the bumps was reversed and heat load data was collected for 15 more minutes.

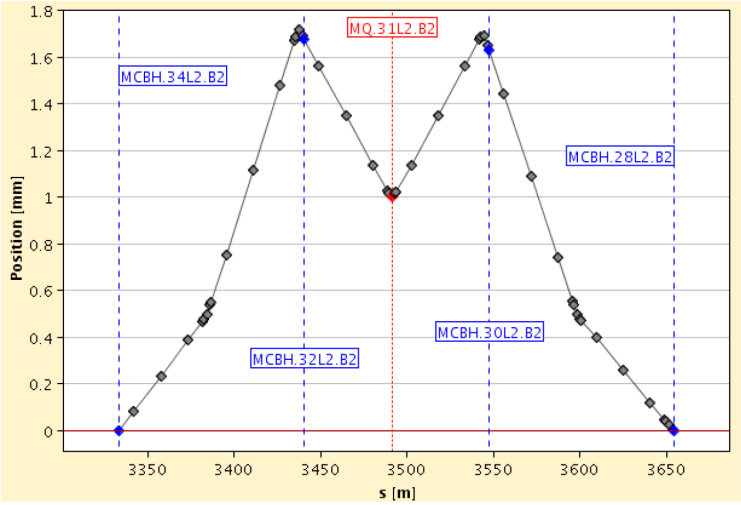

Figure 32: Example of an orbit bump using four corrector magnets.

	H bump	V bump
beam 1	Q23L3, Q29R2, Q13R4, Q33L5 Q29L7, Q23R6, Q27L1, Q23R8	Q31L2, Q25R1, Q31L4, Q25R3 Q21L6, Q17R5, Q25R7, Q21L8
beam 2	Q31L2, Q25R1, Q31L4, Q25R3 Q21L6, Q17R5, Q25R7, Q21L8	Q23L3, Q29R2, Q13R4, Q33L5 Q29L7, Q23R6, Q27L1, Q23R8

Table 2: Quadrupoles at the center of applied orbit bumps.

Figures 33 - 35 show the heat load evolution during the test for the different magnets of three instrumented cells in which the bumps were applied. The total heat loads in other cells in which the bumps were applied are shown in Figs. 36 - 37.

In all cases, no significant effect of the applied bumps is visible on the heat loads. This test allowed excluding orbit differences, magnet misalignments and local losses as the source of cell-by-cell and arc-by-arc differences in heat load. Moreover, the test has proven that the pumping holes on the beam screen are unlikely to be playing a major role, as the beams were significantly displaced compared to hole size and position.

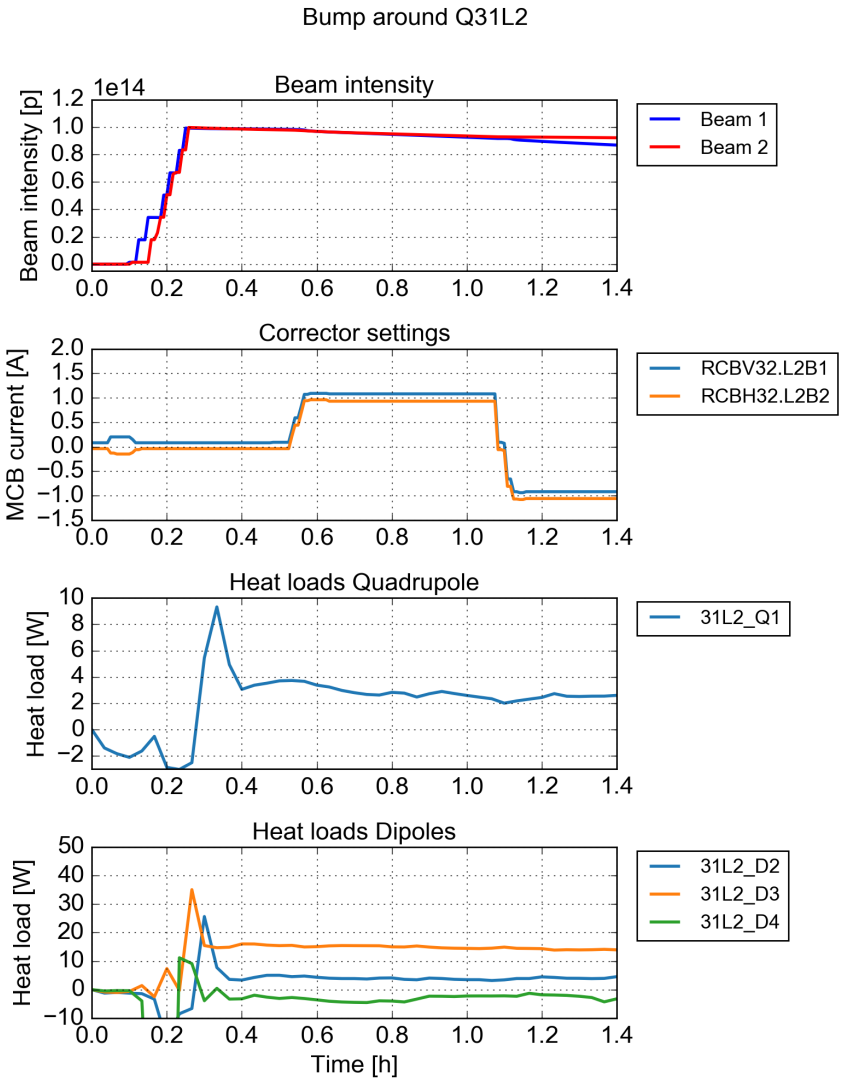

Figure 33: Beam intensities, current in the corrector magnets used to apply the bumps, and heat loads measured in the corresponding instrumented magnets.

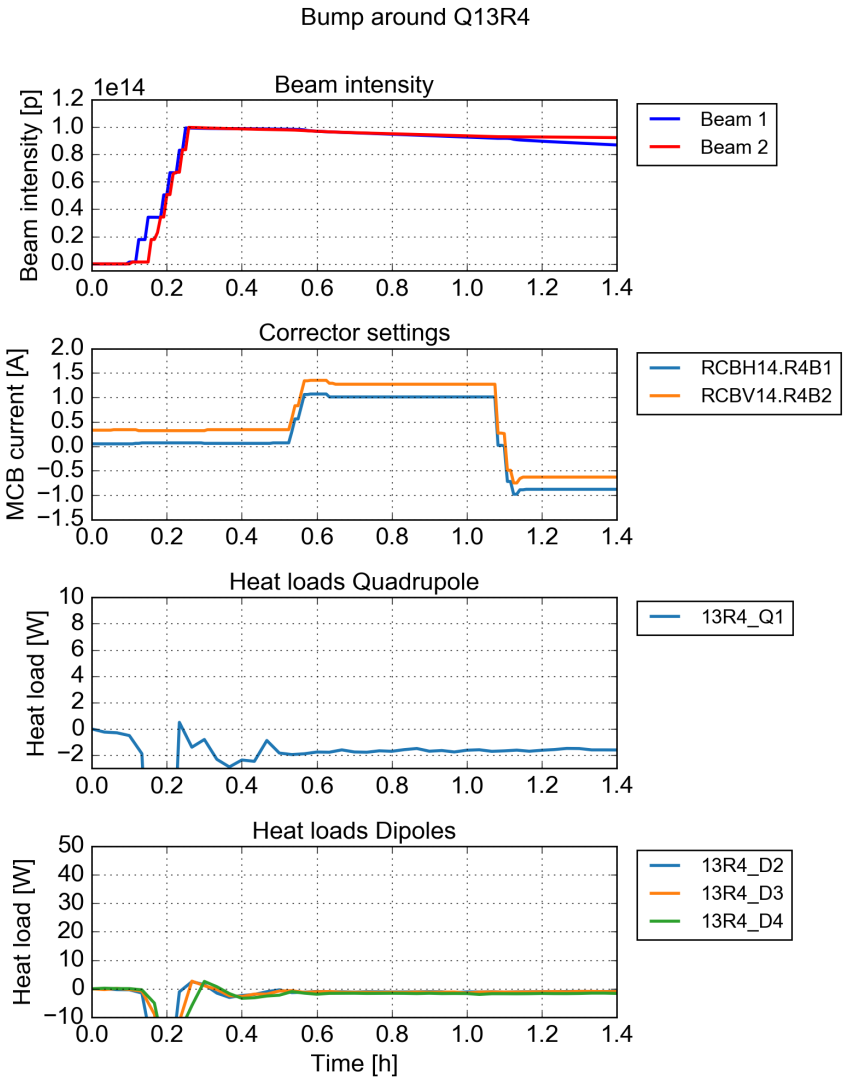

Figure 34: Beam intensities, current in the corrector magnets used to apply the bumps, and heat loads measured in the corresponding instrumented magnets.

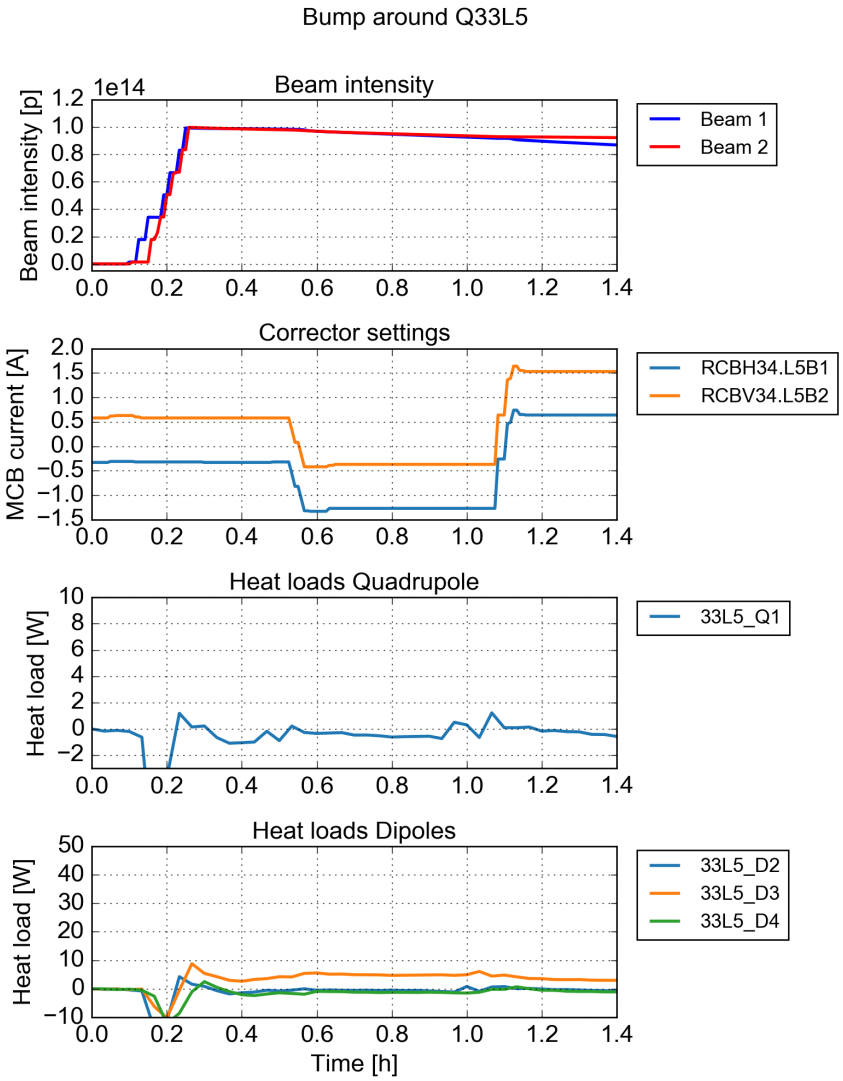

Figure 35: Beam intensities, current in the corrector magnets used to apply the bumps, and heat loads measured in the corresponding instrumented magnets.

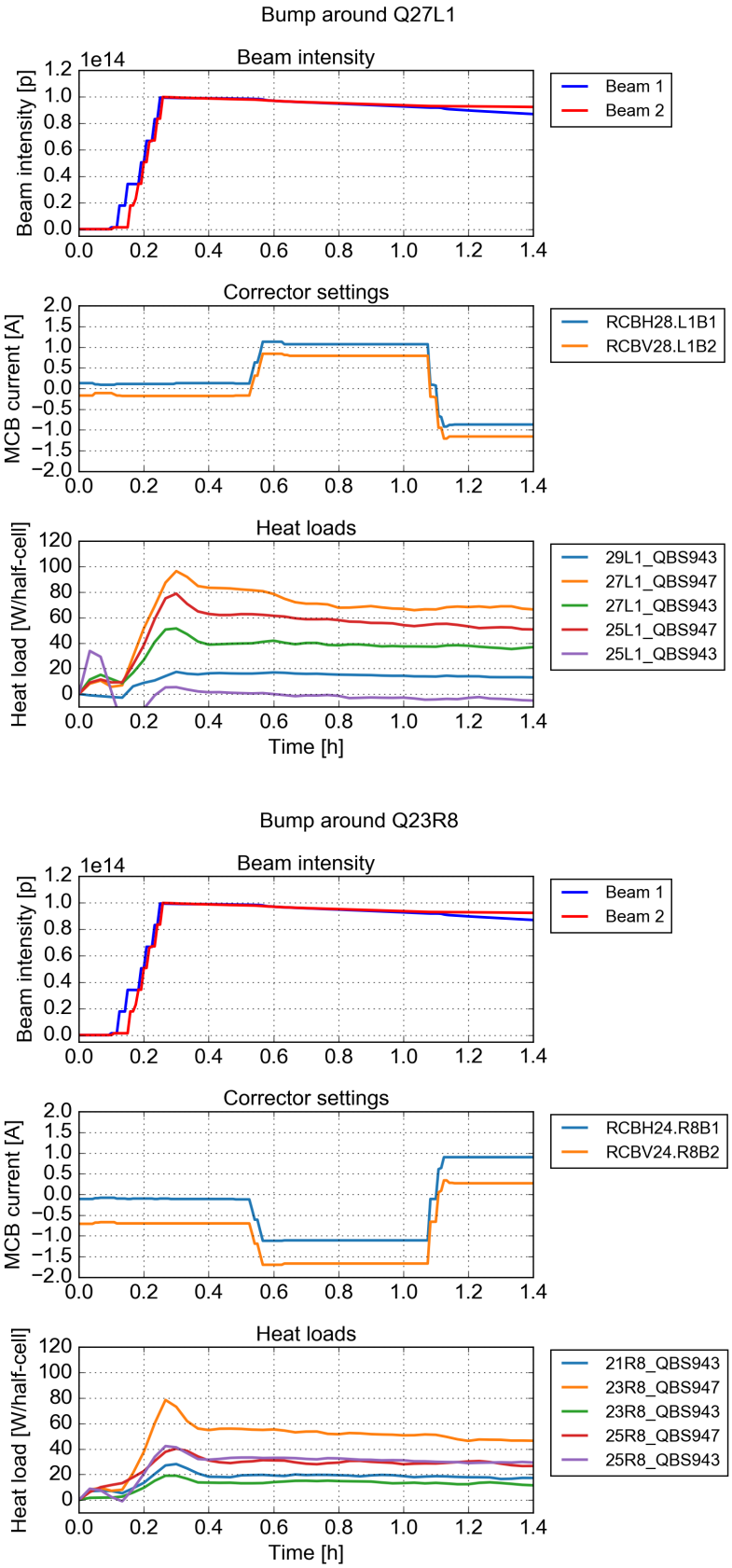

Figure 36: Beam intensities, current in the corrector magnets used to apply the bumps, and heat loads measured in the corresponding half-cells.

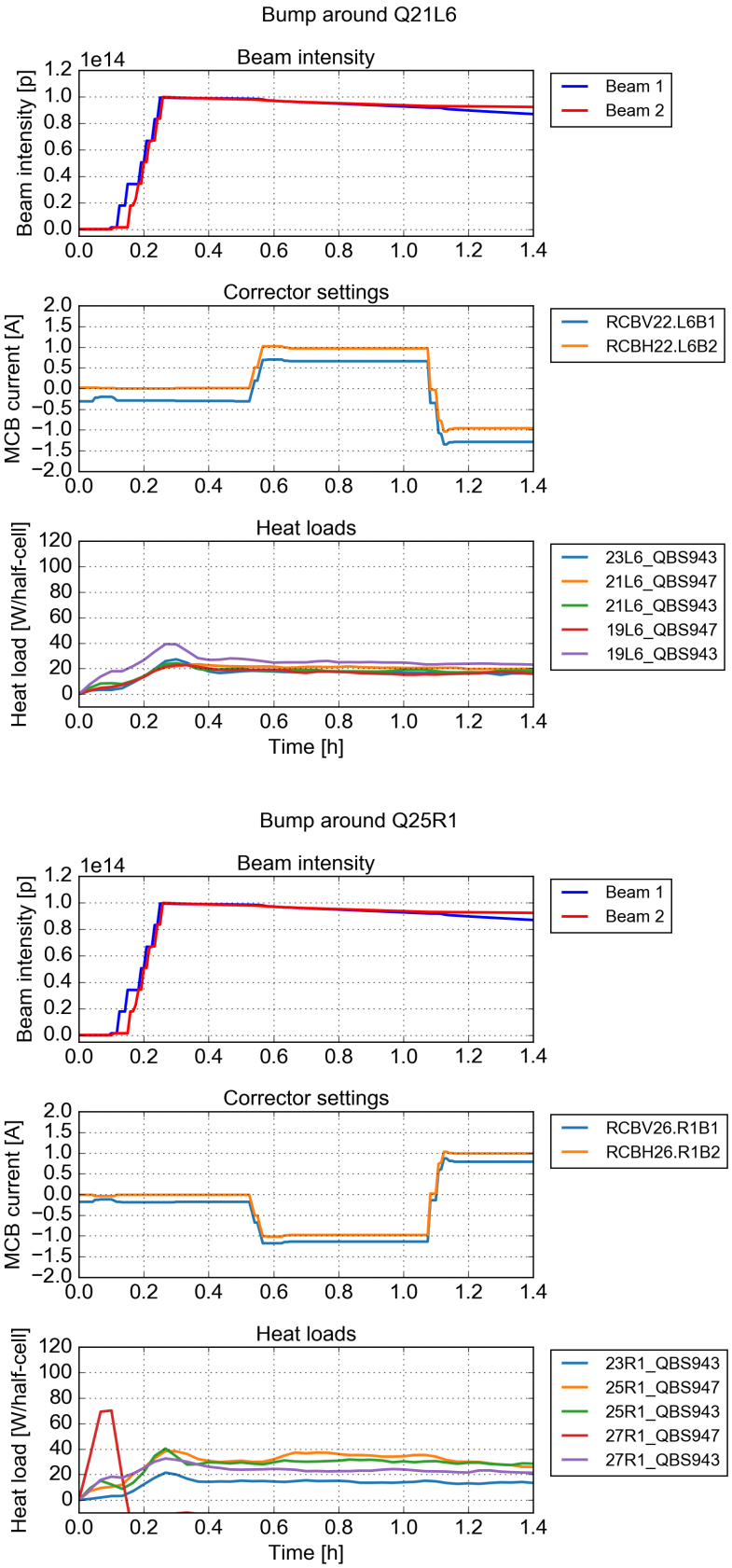

Figure 37: Beam intensities, current in the corrector magnets used to apply the bumps, and heat loads measured in the corresponding half-cells.

3 Comparisons against models and simulations

The experimental observations from the tests illustrated so far, together with those made during regular physics fills, provide important information on the source of the heat loads and in particular of the observed differences among arcs.

Based on these features and on the analysis of the heat load measurement technique, it is possible to exclude that the observed differences result from measurement artifacts [19, 20]. It is also possible to show that the power deposited in the form of the heat load ultimately comes from the beam. To do so, the power lost by the beam is inferred from RF stable phase measurements and it is found to be consistent with heat load measurements from the cryogenics [4].

Figure 38 illustrates different mechanisms that can transfer energy from the beam to the beam screen and their compatibility with the available experimental evidence [19, 20]:

- **Beam losses:** the hypothesis that the differences in heat loads are generated by protons lost on the beam screen, can be easily discarded since the total power associated with beam losses (calculated from beam intensity measurements) only amounts to less than 10% of the measured heat loads.
- **Synchrotron radiation:** the possibility that the observed heat loads are deposited by photons radiated by the beam can also be excluded. In fact, the power from synchrotron radiation is proportional to the beam intensity and independent of the bunch spacing, which is inconsistent with the experimental observations (see for example

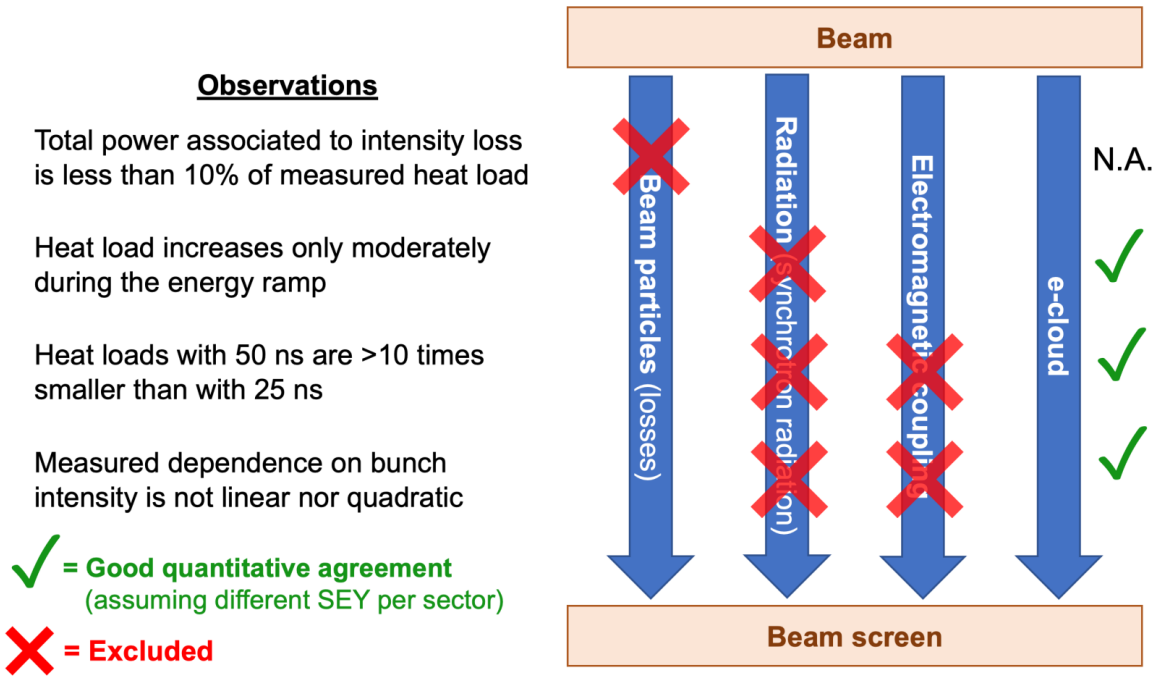

Figure 38: Compatibility of the available experimental observations with different mechanisms transferring power from the beam to the beam screen.

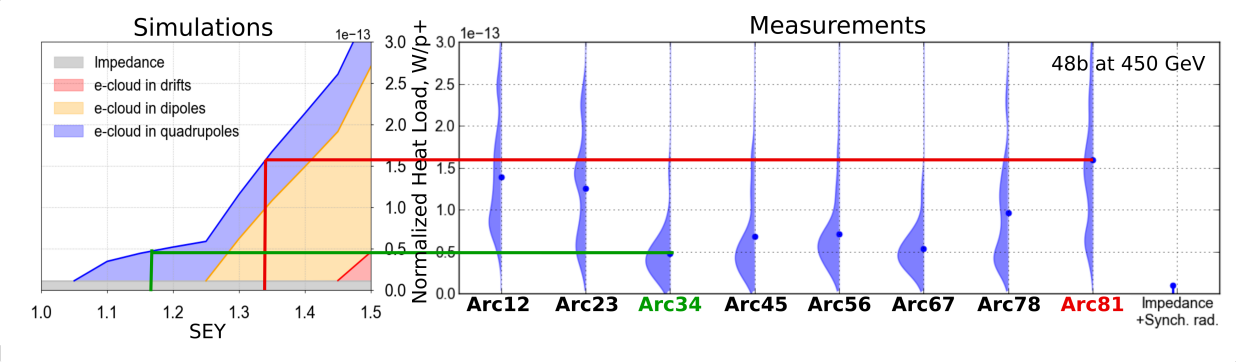

Figure 39: Left: simulated heat load per half-cell as a function of the SEY parameter for two circulating beams at 450 GeV (different contributions are shown in different colors). Right: Corresponding measured heat loads.

Fig. 1). Finally a strong dependence on the beam energy would be expected, while only a small increase is observed during the energy ramp.

- **Beam coupling impedance:** the hypothesis that the energy is transferred through electromagnetic coupling between the beam and the surrounding structures is incompatible with the observations as well. In particular, the measured dependence of the heat load on the bunch intensity is not quadratic (see Fig. 20) and impedance heating cannot justify the large differences observed between 25 ns and 50 ns beams [21]. Moreover, as discussed in Sec. 2.4, impedance heating cannot explain the different dependence of the heat load on the bunch length, which is observed for dipole and quadrupole magnets.

- **Electron cloud effects**: the hypothesis that the energy deposition comes from e-cloud (electrons impacting on the beam pipe) is not in conflict with any of the mentioned observations. It is further investigated by numerical simulations and discussed in the following section.

3.1 Comparison of heat load data against e-cloud simulations

In order to compare the measured heat loads against e-cloud simulations, we assume that the differences observed among arcs and among half-cells are caused by varying surface properties resulting in a different Secondary Electron Yield (SEY) parameter (defined as $\delta_{\max}$ in [22]).

Following this assumption, the e-cloud build-up process has been simulated using the PyECLOUD code [23] as a function of the SEY parameter for all the elements of the LHC arc half-cell. The simulation model is described in detail in [24]. The total simulated heat load as a function of the SEY is shown in Fig. 39 (left) for the two circulating 25 ns beams at 450 GeV, made of trains of 48 bunches. Figure 39 (right) shows the corresponding measured heat loads in the eight arcs. By comparing the two graphs, the SEY parameter corresponding to the average heat load in each arc can be determined, as illustrated in Fig. 39 for the arcs having the largest and the lowest heat loads. Table 3 shows the heat load values inferred in this way from the average heat load of each arc.

Arc	**S12**	**S23**	**S34**	**S45**	**S56**	**S67**	**S78**	**S81**
SEY	1.32	1.30	1.18	1.26	1.26	1.22	1.28	1.34

Table 3: SEY parameters estimated from the average heat load for the different arcs of the LHC.

The same procedure can be applied to the heat load measured at each half-cell, obtaining the corresponding SEY distribution within each arc. Figures 40 - 43 show in blue the cell-by-cell SEY distribution inferred from heat load data measured in 2012 and in red the SEY distribution inferred from data measured in 2018. A significant increase of the SEY is visible in many cells between Run 1 and Run 2, especially in the high-load arcs.

The SEY model defined in this way can be cross-checked against different independent measurements that have been presented in Sec. 2. For this purpose, using the obtained SEY parameters, we simulate the expected heat load as a function of the bunch population for different beam configurations (changing the bunch pattern and the beam energy). Figure 44 shows the simulation results for the operational bunch pattern (trains of 48 bunches) and for the 8b+4e scheme at 6.5 TeV. The dashed curves are calculated assuming uniform SEY along the arcs from Tab. 3. The continuous curves, instead, are calculated assuming for each half-cell the SEY shown in Figs. 40 - 43. The measured data for both beam configurations are shown by the markers in Fig. 44. The high-intensity point for the 8b+4e scheme is obtained from the test described in Sec. 2.5, the other points were measured during physics fills in 2017 and 2018. The agreement between measurements and simulations is found to be very good, especially for the arcs showing the highest heat load.

Systematic comparisons have been performed also at injection energy, as shown in Fig. 45, using measurements taken with the operational bunch pattern and with trains of 12 bunches which allowed probing higher bunch intensities (as described in Sec. 2.3). Also in this case the agreement between simulation and measurements is very good.

It is worth remarking explicitly that the simulation prediction of a small increase of the heat load above 1.0×10^{11} p/bunch is confirmed experimentally both by the test conducted with trains of 12 bunches at 450 GeV and by the test conducted with the 8b+4e beams at high energy.

In general, it is possible to conclude that, not only is e-cloud heating the only identified mechanism that cannot be excluded based on the available observations, but it also allows achieving a good quantitative agreement between measurements and models, when assuming that the root cause of the differences in heat load is a difference in SEY.

During the LHC Long Shutdown 2 in 2019, beam screens have been extracted from low-load and high-load dipole magnets and undergone surface analysis. It was found that, exclusively on the beam screens from the high-load magnets, cupric oxide (CuO) was present, as opposed to the native cuprous oxide (Cu_2O) which is typically found on these surfaces. Moreover the beam screens from the high-load magnets showed an extremely low concentration of carbon. These modifications have been associated with modifications of the SEY and of the conditioning behaviour. The mechanisms leading to these surface alterations are presently being investigated [25, 26].

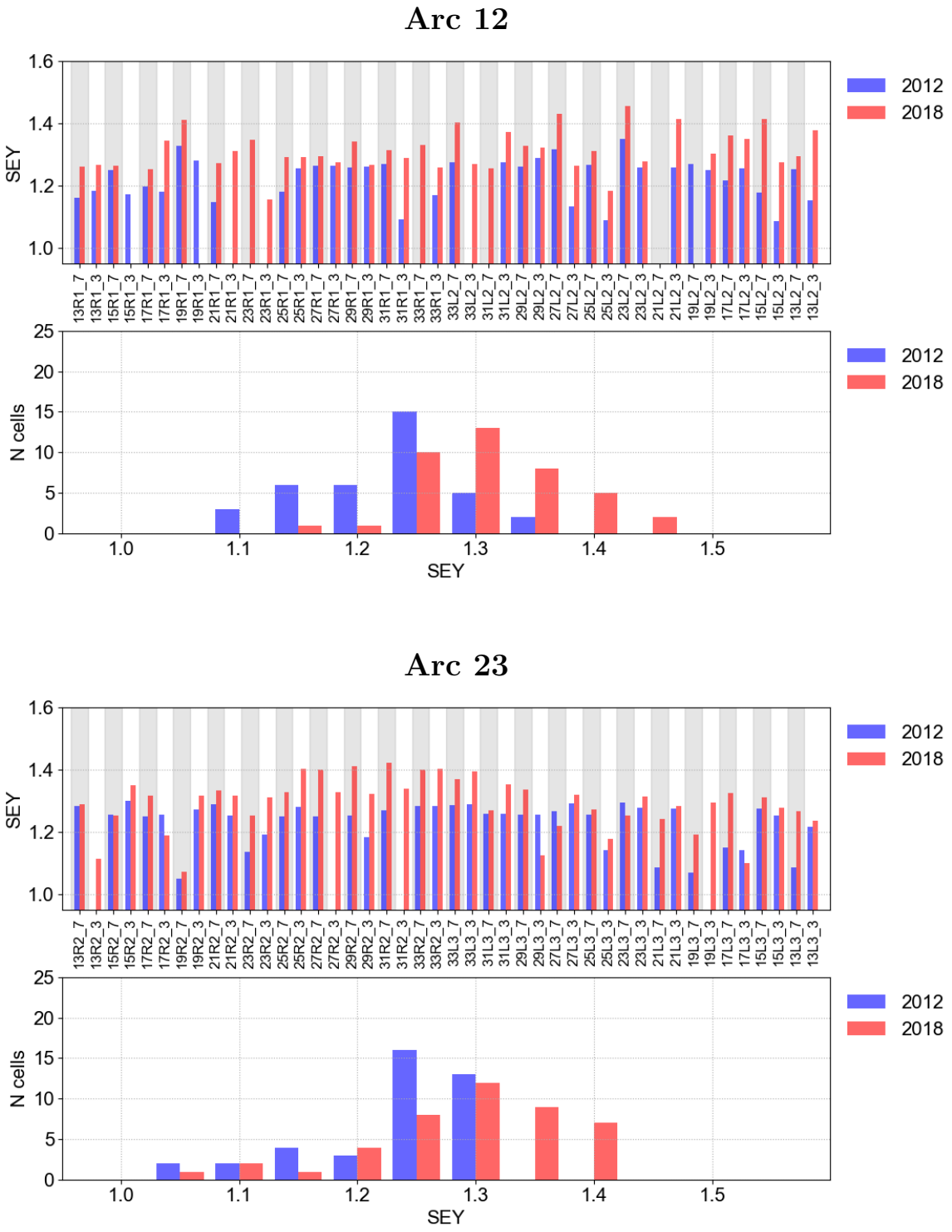

Figure 40: SEY parameter estimated for the cells in the arcs 12 and 23 based on heat loads measured in 2012 (fill 3438) and in 2018 (fill 6786).

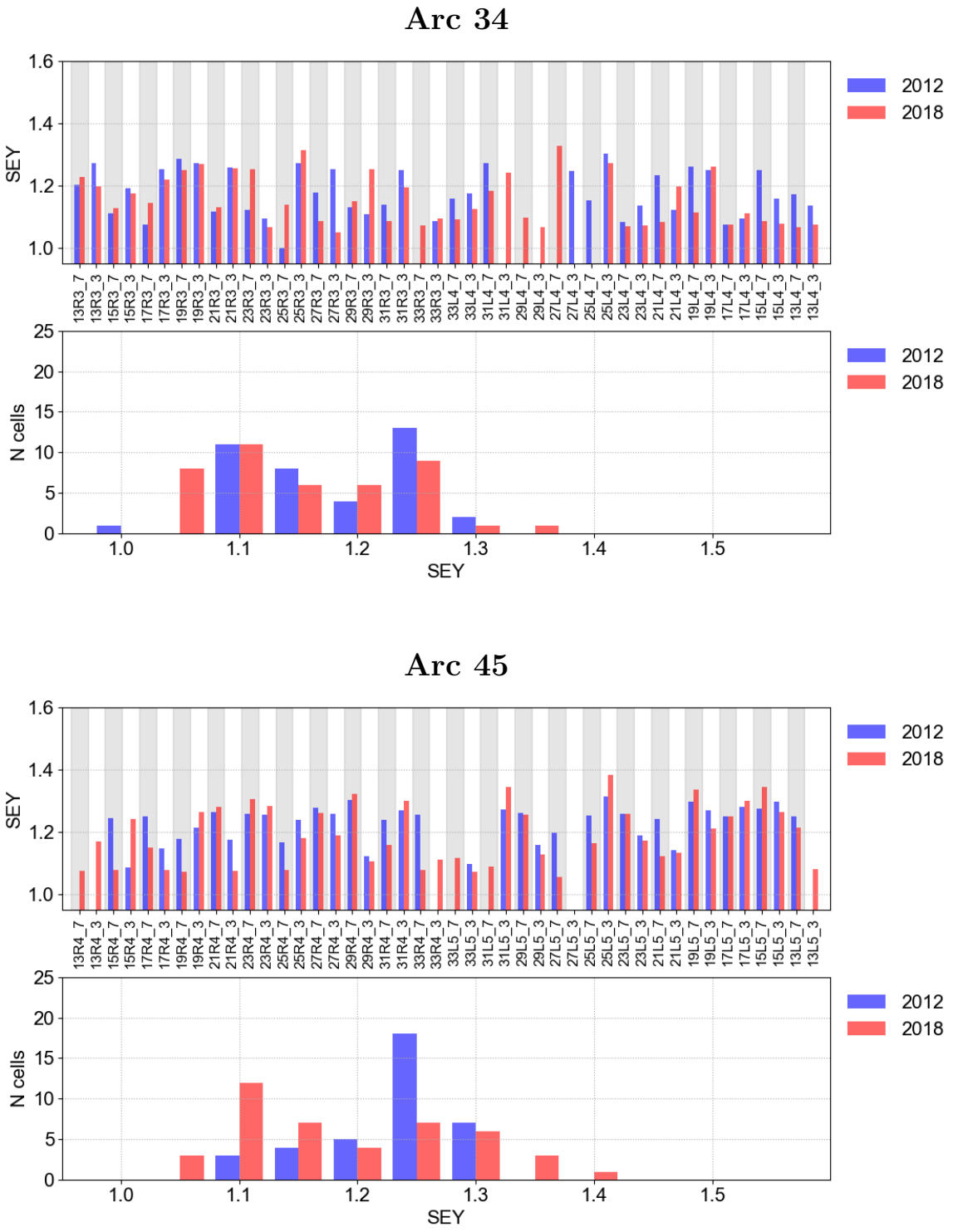

Figure 41: SEY parameter estimated for the cells in the arcs 34 and 45 based on heat loads measured in 2012 (fill 3438) and in 2018 (fill 6786).

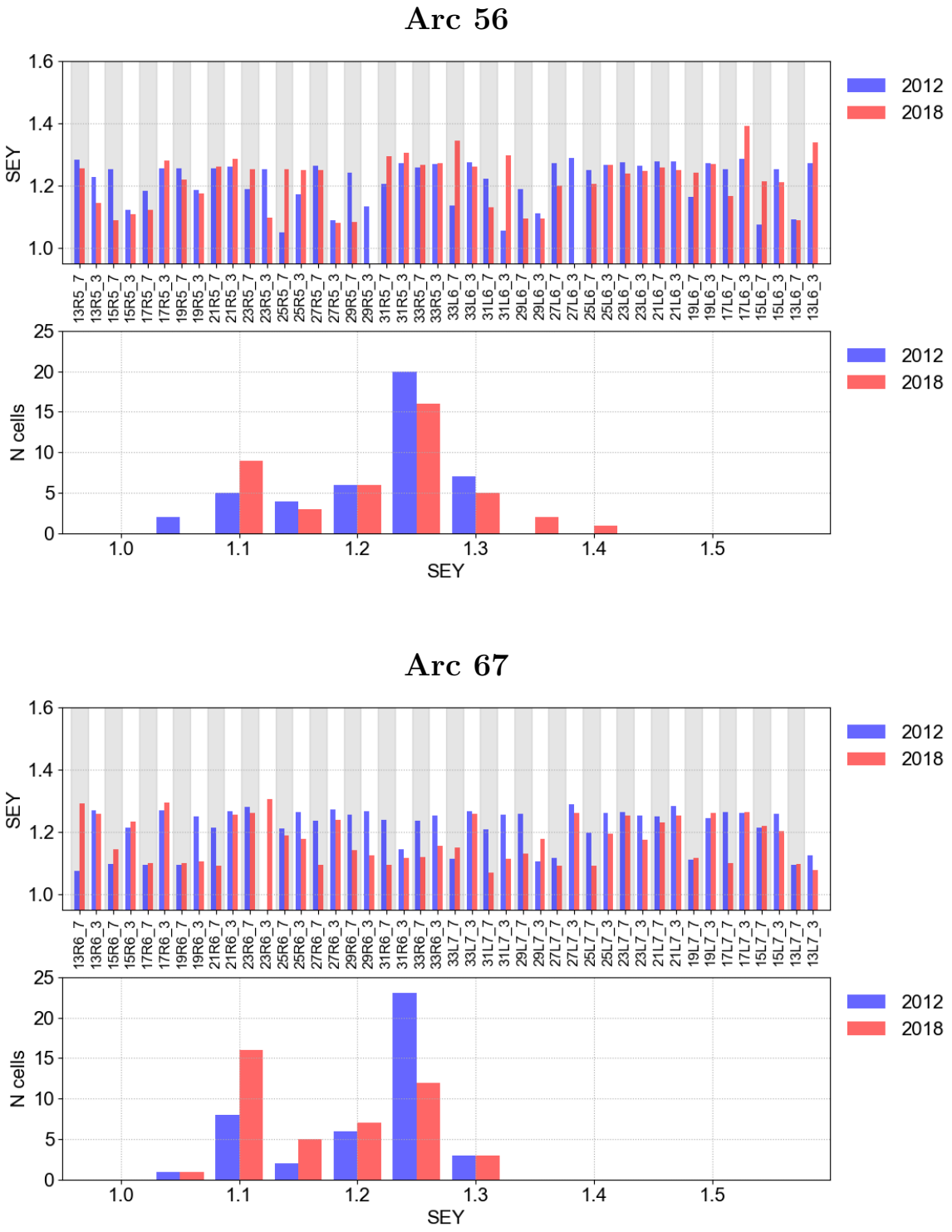

Figure 42: SEY parameter estimated for the cells in the arcs 56 and 67 based on heat loads measured in 2012 (fill 3438) and in 2018 (fill 6786).

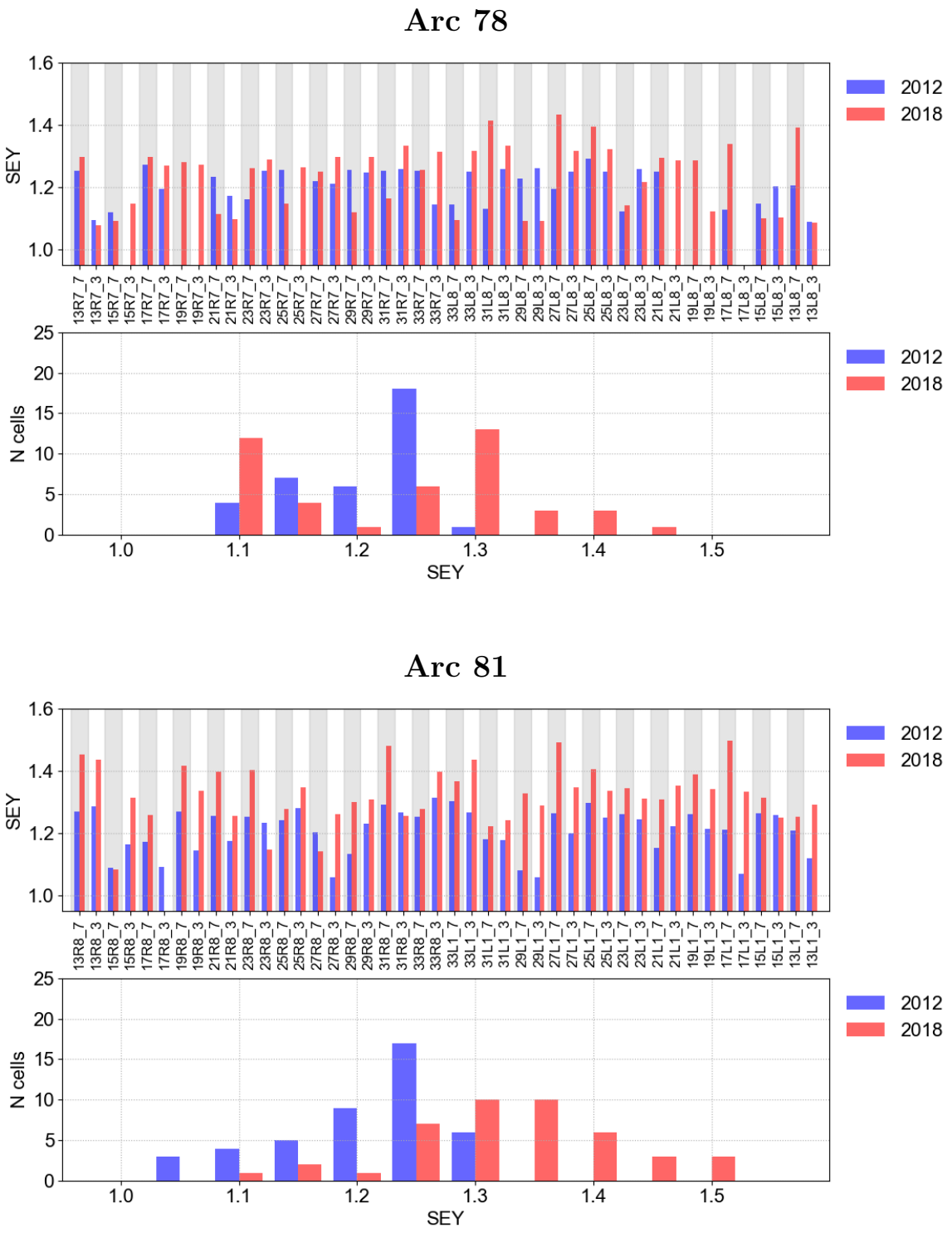

Figure 43: SEY parameter estimated for the cells in the arcs 78 and 81 based on heat loads measured in 2012 (fill 3438) and in 2018 (fill 6786).

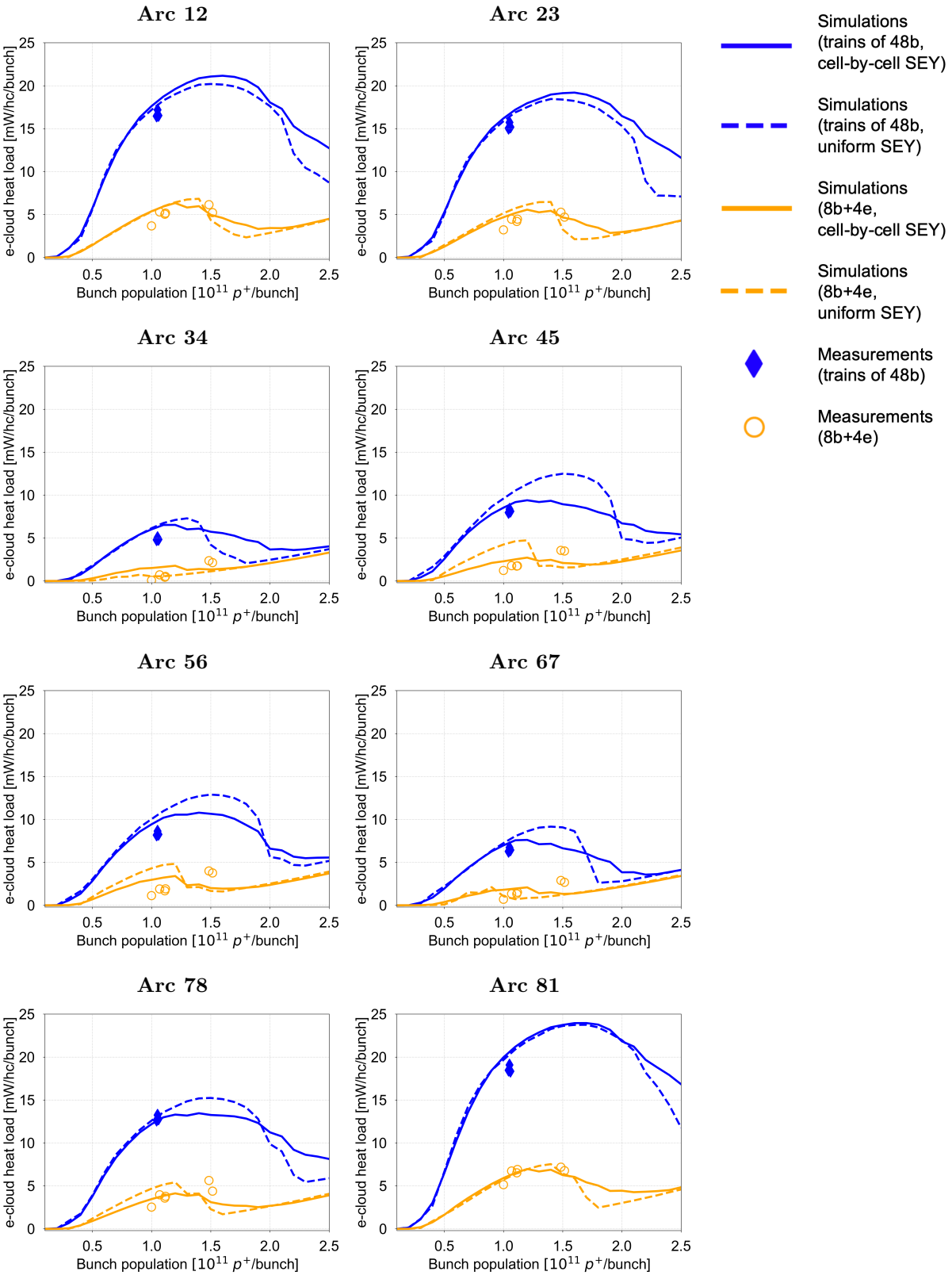

Figure 44: Comparison of the simulated and measured heat loads for different beam configurations at 6.5 TeV. The SEY values used here are inferred from the data points marked by red circles in Fig. 45.

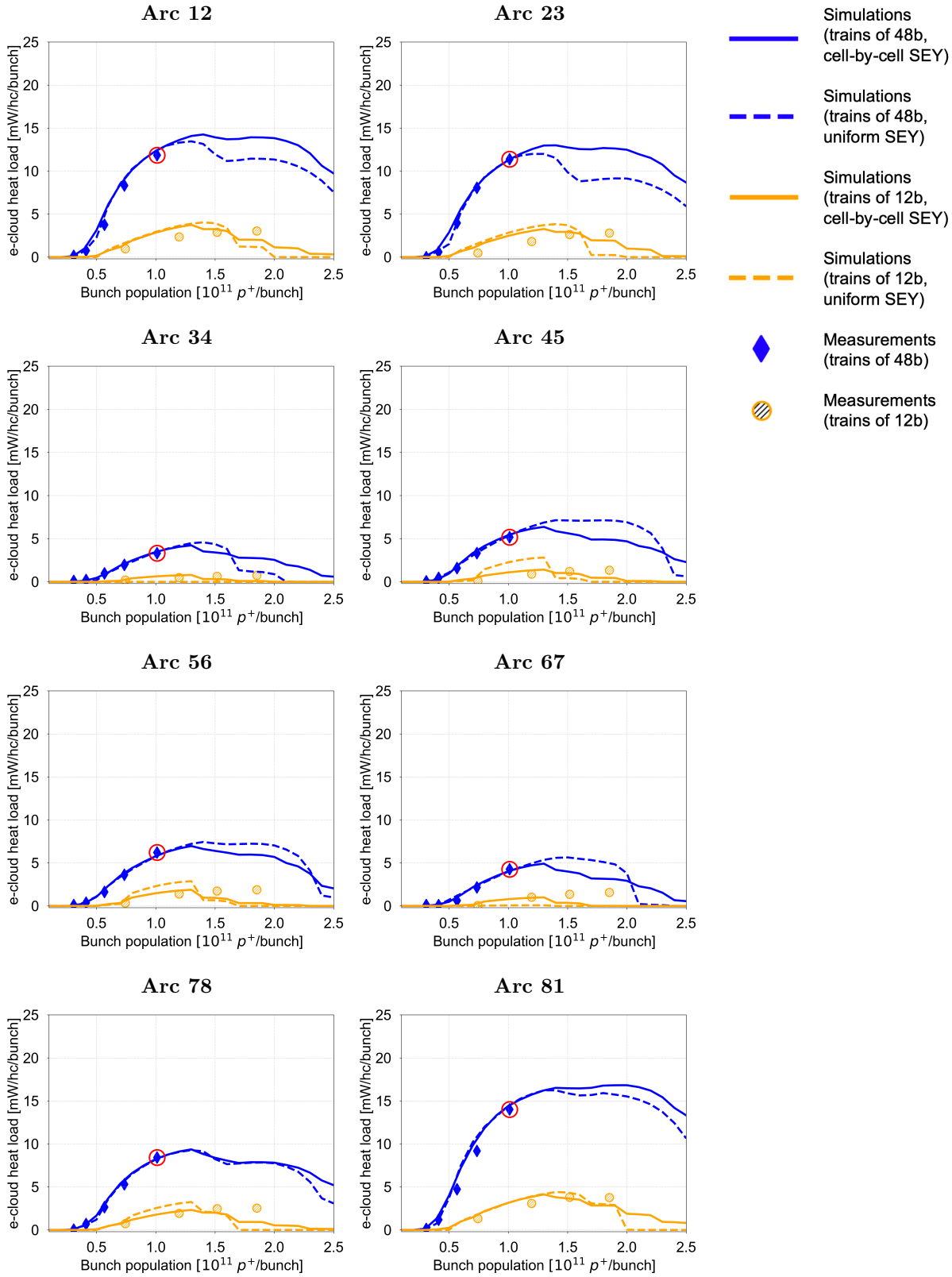

Figure 45: Comparison of the simulated and measured heat loads for different beam configurations at 450 GeV. The red circles mark the data points used to infer the SEY parameters.

4 Conclusions

The heat loads deposited by electron cloud on the LHC arc beam screens and in particular the differences observed among the eight LHC arcs have been investigated with different experimental tests during MD sessions in 2018. The main findings of these studies can be summarized as follows:

- By performing fills with a single circulating beam it was possible to show that both beams contribute in a similar manner to the total heat load in each arc. Nevertheless, in several cells significant differences between the two beams can be observed. From the special instrumented cells it is possible to observe that in some magnets differences are present even between the two apertures of the same magnet.

- Using injections of 3×48 bunches, it was found that the dependence of the heat loads on the number of circulating bunches is practically linear for all arcs.

- When changing the bunch intensity, it was found that the heat load from e-cloud becomes measurable only above a certain bunch intensity of about 0.4×10^{11} p/bunch.

- Using short bunch trains of 12 bunches it was possible to probe the dependence of the heat loads on the bunch intensity up to 1.9×10^{11} p/bunch. It was observed that above 1.5×10^{11} p/bunch the heat load produced by e-cloud tends to saturate and even slightly decreases. Also using 8b+4e beams it was observed that increasing the bunch intensity from 1.1×10^{11} p/bunch to 1.5×10^{11} p/bunch the observed heat load increase is quite modest.

- The dependence of the heat loads on the bunch intensity was also investigated with dedicated measurements. The dipole magnets showed a reduction of the heat load when the bunch length is increased. The quadrupole magnets, instead, show the opposite behaviour with the heat load increasing when the bunch length is increased. Such different behaviour for dipole and quadrupole magnets is expected for e-cloud effects, while it is incompatible with other heating mechanisms, and in particular with impedance heating.

- Additional tests showed that there is no effect on the heat loads when applying orbit bumps as large as four millimetres nor when changing the settings of the spool-piece correctors.

The SEY parameter could be inferred for all the arc half-cells by comparing the heat load measured at 450 GeV with the operational 25 ns beam configuration against e-cloud buildup simulations. The model built in this way was used to simulate the e-cloud buildup for different beam configurations as a function of the bunch intensity. The heat load calculated in this way could be compared against the measurements collected during the experimental tests, finding very good agreement.

References

[1] G. Iadarola, G. Rumolo, P. Dijkstal, and L. Mether, "Analysis of the beam induced heat loads on the LHC arc beam screens during Run 2," *CERN-ACC-NOTE-2017-0066*, Dec 2017.

[2] G. Iadarola *et al.*, "Electron cloud and heat loads in Run 2," *in Proc. 2019 Evian Workshop on LHC beam operation, Evian Les Bains, France*, Jan 2019. https://indico.cern.ch/event/751857/.

[3] G. Apollinari, I. Bejar Alonso, O. Bruning, P. Fessia, M. Lamont, L. Rossi, and L. Tavian, *High-Luminosity Large Hadron Collider (HL-LHC): Technical Design Report V. 0.1*. CERN Yellow Reports: Monographs 4/2017, Geneva: CERN, 2017.

[4] G. Iadarola, "Head loads in Run 1 and Run 2," *Presentation at the LHC Machine Committee, CERN*, 12 Sep 2018. https://indico.cern.ch/event/756722/.

[5] L. Tavian, "Report from the task force on beam induced heat load," *Presentation at the LHC Performance Workshop 2018, Chamonix*, Jan 2018. https://indico.cern.ch/event/676124/.

[6] G. Iadarola, "Beam lifetime in collision - LHC experience," *Presentation at the 160th HL-LHC WP2 meeting, CERN*, 24 Sep 2019. https://indico.cern.ch/event/850136/.

[7] G. Iadarola, "Analysis of the heat load differences among sectors," *Presentation at the 46th Electron Cloud Meeting, CERN*, 25 Aug 2017. https://indico.cern.ch/event/660465/.

[8] G. Skripka and G. Iadarola, "Beam-induced heat loads on the beam screens of the HL-LHC arcs," *CERN-ACC-NOTE-2019-0041*, Oct 2019.

[9] H. Bartosik, G. Iadarola, G. Rumolo, F. Caspers, M. Driss Mensi, S. Federmann, M. Holz, H. Neupert, and M. Taborelli, "Electron Cloud and Scrubbing Studies for the SPS in 2012," *CERN-ATS-NOTE-2013-019 MD*, Apr 2013.

[10] H. Bartosik *et al.*, "Injectors peam performance evolution during run 2," *in Proc. 2019 Evian Workshop on LHC beam operation, Evian Les Bains, France*, Jan 2019. https://indico.cern.ch/event/751857/.

[11] G. Rumolo *et al.*, "What to expect from the injectors during run 3," *in Proc. 2019 Evian Workshop on LHC beam operation, Evian Les Bains, France*, Jan 2019. https://indico.cern.ch/event/751857/.

[12] X. Buffat *et al.*, "Transverse instabilities," *in Proc. 2019 Evian Workshop on LHC beam operation, Evian Les Bains, France*, Jan 2019. https://indico.cern.ch/event/751857/.

[13] A. Romano, O. Boine-Frankenheim, X. Buffat, G. Iadarola, and G. Rumolo, "Electron cloud buildup driving spontaneous vertical instabilities of stored beams in the Large Hadron Collider," *Phys. Rev. Accel. Beams*, vol. 21, p. 061002, Jun 2018.

[14] G. Iadarola, "200 MHz Scenario: e-cloud," *Presentation at the 68th HL-LHC WP2 meeting, CERN*, 3 May 2016.
https://indico.cern.ch/event/523881/timetable/.

[15] G. Iadarola, H. Bartosik, K. Li, L. Mether, A. Romano, G. Rumolo, and M. Schenk, "Performance limitations from electron cloud in 2015," *in Proc. of 6th Evian Workshop on LHC beam operation, Evian Les Bains, France*, pp. 101–110, Dec 2015.

[16] L. Mether, D. Amorim, G. Arduini, X. Buffat, G. Iadarola, D. Mirarchi, G. Rumolo, and B. Salvant, "16L2: operation, observations and physics aspects," *in Proc. of the 8th LHC Operations Evian Workshop, Evian Les Bains, France*, Dec 2017.

[17] S. Fartoukh *et al.*, "Round telescopic optics with large telescopic index," *CERN-ACC-2018-0032*, Sep 2018.

[18] "FiDeL home: the Field Model of the LHC."
http://lhc-div-mms.web.cern.ch/lhc-div-mms/tests/MAG/Fidel/.

[19] G. Iadarola, "Electron cloud and heat loads in the LHC arcs," *Presentation at the Accelerator and beam physics forum, CERN*, 12 Jul 2018.
https://indico.cern.ch/event/740046.

[20] G. Iadarola, "Heat loads in the LHC arcs: observations and comparison against models," *Presentation at the LHC Machine Committee, CERN*, 29 Aug 2018.
https://indico.cern.ch/event/754131/.

[21] B. Salvant and F. Giordano, "Impedance considerations," *Presentation at the 46th Electron Cloud Meeting, CERN*, 25 Aug 2017.
https://indico.cern.ch/event/660465/.

[22] R. Cimino, I. R. Collins, M. A. Furman, M. Pivi, F. Ruggiero, G. Rumolo, and F. Zimmermann, "Can low-energy electrons affect high-energy physics accelerators?," *Phys. Rev. Lett.*, vol. 93, p. 014801, Jun 2004.

[23] G. Iadarola, E. Belli, K. Li, L. Mether, A. Romano, and G. Rumolo, "Evolution of python tools for the simulation of electron cloud effects," *in Proc. 8th International Particle Accelerator Conference, Copenhagen, Denmark*, May 2017. pp.THPAB043.

[24] P. Dijkstal, G. Iadarola, L. Mether, and G. Rumolo, "Simulation studies on the electron cloud build-up in the elements of the LHC Arcs at 6.5 TeV," *CERN-ACC-NOTE-2017-0057*, Oct 2017.

[25] V. Petit, "Update on LHC beam screen analysis," *https://indico.cern.ch/event/523881/timetable/ the 69th Electron Cloud Meeting, CERN*, 14 Aug 2019.
https://indico.cern.ch/event/835473/.

[26] M. Taborelli, "Heat load task force: outcome of the analysis of beam screens and implications," *Presentation at the LHC Machine Committee, CERN*, 2 Oct 2019. https://indico.cern.ch/event/852492/.